REPORT SERIES IN PHYSICS
HU-P-D254

UNIVERSITY OF HELSINKI

Novel Detector Technologies for Medical Applications at the Example of Tumor Detection in BNCT

Author:
Alexander Dieter
WINKLER

Supervisor:
Prof. Dr. Sauli
SAVOLAINEN

Department of Physics
Faculty of Science
and Helsinki Institute of Physics

ACADEMIC DISSERTATION

To be presented for public criticism, with the permission of the Faculty of Science of the University of Helsinki, in the auditorium D101 of the Physicum building, Gustaf Hällströmin katu 2a, on Friday, October 20th, 2017, at 12:00 o'clock.

Helsinki, 2017

Supervisor:
Prof. Sauli Savolainen, Ph.D.
Department of Physics
University of Helsinki
Finland

Reviewers:
Prof. Ari Virtanen, Ph.D.
Research director RADEF facility
University of Jyväskylä
Finland

Adj. Prof. Jani Keyriläinen, Ph.D.
Medical Physics
Turku University Hospital
Finland

Opponent:
Prof. Ari Jokinen, Ph.D.
Department of Physics
University of Jyväskylä
Finland

ISBN 978-951-51-3691-6 (Paperback)
ISSN 0356-0961
Helsinki University Print (Unigrafia OY)
Helsinki 2017

ISBN 978-951-51-3692-3 (PDF)
http://ethesis.helsinki.fi
Electronic Publications at the University of Helsinki
Helsinki 2017

"No government has the right to decide on the truth of scientific principles, nor to prescribe in any way the character of the questions investigated. [...] Instead it [the government] has a duty to its citizens to maintain the freedom, to let those citizens contribute to the further adventure and the development of the human race."

Richard Feynman

University of Helsinki

Abstract

Faculty of Science
Department of Physics
Faculty of Science
and Helsinki Institute of Physics

Doctor of Philosophy

Novel Detector Technologies for Medical Applications at the Example of Tumor Detection in BNCT

by Alexander Dieter WINKLER

The next evolutionary step in medical imaging and radiation therapy is to employ novel detector technologies capable of photon counting operations. These detectors allow to acquire the spectrum of the radiation for each pixel. Currently used energy integrating detectors do not allow this. Two types of detector materials capable of photon counting operation are discussed in this work. With the result that the detector technology based on CdTe and CdZnTe is more matured than GaAs. The spectral information of photon counting detectors can be used for numerous applications and diagnostic improvements. A distinct example is presented for boron neutron capture therapy (BNCT). This therapy lacks an accurate real time method to determine the ^{10}B concentration within the patient. Previous approaches failed because of the low signal to noise ratio of the used signal. A method has been proposed to improve this therapy by employing CdTe based photon counting detectors. These detectors allow detection of a secondary signal with a higher signal to noise ratio. Additionally, efforts to produce CdTe based photon counting detector arrays, for medical applications, are described.

Acknowledgements

A PhD thesis is in most cases a group work, therefore it is my deepest desire to acknowledge the people that have in one way or the other contributed to this process.

I wish to thank the Department of Physics at the University of Helsinki, the Helsinki Institute of Physics (HIP) and it's Detector Laboratory for providing the resources and the framework for the research that is presented in this thesis.

In particular, I wish to that Prof. Sauli Savolainen who kindly accepted me to the medical physics studies within the Doctoral Programme in Materials Research and Nanosciences (MATRENA) and is continuing to provide invaluable support for the continuation of the long path towards the hospital physicist. I am equally indebted to Dr. Jaakko Häkönen for accepting me to the CMS upgrade project, even though my official studies were not within the Doctoral Programme of Particle Physics and Universe Sciences (PAPU). He saw the synergy that the both fields — medical- and particle physics — can gain, when working together. For this and the guidance that he and later Dr. Panja Luukka kindheartedly granted, I am most grateful.

On the research side, I owe my thanks to Dr. Hanna Koivunoro who has taken the time to plan, realize and improve our research in countless discussions. She is one of the few people that has endured these discussions from the beginning. Similarly, I like to thank Iiro Auterinen for his support and his creative input.

At the Detector laboratory of HIP, I like to thank Dr. Eija Tuominen and the laboratory engineers Jouni Heino and Raimo Turpeinen for helping to organize the needed resources and to solve problems quickly. Similarly, our colleague Rauno Lauhakangas, will always have my innermost gratitude for teaching immeasurable knowledge about detectors, a sustainable way of thinking and the many cheerful discussions.

I sincerely thank my colleagues Dr. Jaakko Häkönen, Dr. Panja Luuka and Dr. Erik Brücken for their helpful suggestions and comments that improved this thesis and it's contend substantially. Equally, I thank Adj. Prof. Jani Keyrilainen and Prof. Ari Virtanen for their agreement to conduct the pre-examination of this thesis. Their numerous comments helped to focus the

message I like to convey. Furthermore, I like to thank Donald Smart for providing the language review.

The research related travels and other support was partially provided by the MATRENA doctoral programme, for which I am grateful. Special thanks are owed to PharmD. Alma Kartal-Hodzic for her ever open ear to solve the little problems of doctoral students.

On a personal level I like to thank my friends and colleagues Dr. Erik Brücken, Dr. Aneliya Karadzhinova-Ferrer and Tiina Naaranoja for their motivation, distractions, the vast amounts coffee and their shoulders to cry on. Finally, I wish to thank my family and friends for their endless support on this part of my journey.

For Birgitt.

Contents

List of Figures

List of Tables

List of Original Publications

I Alexander Winkler, Hanna Koivunoro, Vappu Reijonen, Iiro Auterinen, and Sauli Savolainen (2015). "Prompt gamma and neutron detection in BNCT utilizing a CdTe detector". In: *Applied Radiation and Isotopes* 106, pp. 139–144. DOI: http://dx.doi.org/10.1016/j.apradiso.2015.07.040

II Alexander Winkler, Hanna Koivunoro, and Sauli Savolainen (2017a). "Analysis of MCNP simulated gamma spectra of CdTe detectors for Boron Neutron Capture Therapy". In: *Applied Radiation and Isotopes* 124, pp. 114–118. DOI: http://dx.doi.org/10.1016/j.apradiso.2017.03.018

III Alexander Winkler, Hanna Koivunoro, Iiro Auterinen, and Sauli Savolainen (2017b). "Evaluation of a method to localize ^{10}B in a phantom with a CdTe spectrometer for Boron Neutron Capture Therapy". In: *Journal of Instrumentation*. Under review.

IV X Wu, T Peltola, T Arsenovich, A Gädda, J Härkönen, A Junkes, A Karadzhinova, P Kostamo, H Lipsanen, P Luukka, M Mattila, S Nenonen, T Riekkinen, E Tuominen, and A Winkler (2015). "Processing and characterization of epitaxial GaAs radiation detectors". In: *Nuclear Instruments and Methods in Physics Research Section A: Accelerators, Spectrometers, Detectors and Associated Equipment* 796, pp. 51–55. DOI: http://dx.doi.org/10.1016/j.nima.2015.03.028

V S. Spannagel on behalf of CMS Tracker Collaboration (2017). "Test Beam Performance Measurements for the Phase I Upgrade of the CMS Pixel Detector". In: *Journal of Instrumentation* 12 (05), P05022. DOI: 10.1088/1748-0221/12/05/P05022

The author (Alexander Dieter WINKLER) has coordinated and participated in the experimental work for Publications I - III, he was supported by the co-authors of Publication I and III. All of the analytic work and the result presentation has been carried out by the author for Publications I - III. The formation of the idea of the proposed modification for BNCT-SPECT, was done in cooperation with the co-author Iiro Auterinen. Furthermore, all of the simulations were performed by the author for all, but Publications IV and V. The author has also written the manuscripts for Publications I - III. The contribution by the co-authors for Publications I - III were guidelines to results interpretation, improvements on the explanatory content as well as suggestions for additional topics of investigation.

The author's contributions to Publication IV were assistance in the design and preparation of the PCB boards, on which the GaAs detectors were tested with the TCT-setup at HIP. Furthermore, substantial efforts were undertaken by the author, to reduce the electrical noise of the TCT-setup, in order to allow the recording of the published data. Finally, the author contributed actively to the manuscript writing process.

Publication V is a report by Simon Spannagel and the CMS Tracker community, of which the author is a member. The report discusses the full system quality assurance, functionality and the technical verification, the performance and capabilities of the new pixel readout CMOS ASIC chip of the CMS pixel tracker. The authors contribution to Publication V and the CMS Phase I Upgrade -project was to set up and test the measurement system, necessary to perform the verification of the pixel detector modules that were produced at HIP. These modules are now installed in the CMS experiment at LHC, CERN. In addition, electrical measurements for a large quantity of these modules were performed. The measurements were essential for the determination and replacement of malfunctioning detectors. This allowed HIP to deliver its contractual agreed number of detector modules to the CMS project in time and on budget. The

author's position in the author list of Publication V follows the common practise for publications of large collaborations and is determined by the alphabetical orders of the countries, institutions and contributing members of the institutions.

List of Abbreviations

ALARA	**A**s **L**ow **A**s **R**easonably **A**chievable
As	**Ar**s**e**nic
B	**B**oron
BM	**B**ridgman **M**ethod growth
BNC	**B**oron **N**eutron **C**apture
BNCT	**B**oron **N**eutron **C**apture **T**herapy
BPA	**B**orono**p**henyl**a**lanine
^{10}**B(n,**α**)**^{7}**Li***	BNC reaction equation (the asterisk is usually omitted)
C	**C**zochralski growth
Cd	**Ca**d**m**ium
CdNC	**Ca**d**m**ium **N**eutron **C**apture
CdTe	**Ca**d**m**ium **Te**lluride
CERN	**C**onseil **E**uropéenne pour la **R**echerche **N**ucléaire
CMS	**C**ompact **M**uon **S**olenoid
CT	**C**omputed **T**omography
CVD	**C**hemical **V**apor **D**eposition growth
CVPE	**C**hloride **V**apor **P**hase **E**pitaxy growth
^{113}**Cd(n,**γ**)**^{114}**Cd***	CdNC reaction equation
emis	**emis**sion
eV	**e**lectron **V**olt
F4	Tally **F**4
F8	Tally **F**8
FWHM	**F**ull **W**idth at **H**alf **M**aximum
Ga	**Ga**llium
GaAs	**Ga**llium **Ar**s**e**nide
Ge	**Ge**rmanium
HIP	**H**elsinki **I**nstitute of **P**hysics
HPB	**H**igh-**P**ressure **B**ridgman growth
ILO	**I**nternational **L**abour **O**rganization
IR	**I**nfra**r**ed
LEC	**L**iquid **E**ncapsulated **C**zochralski growth

LHC	**L**arge **H**adron **C**ollider
MC	**M**onte **C**arlo
MCNP	**M**onte **C**arlo **N**-**P**article Transport code
NCT	**N**eutron **C**apture **T**herapy
PC	**P**hoton **C**ounting
PE	**P**oly**e**thylene
PET	**P**ositron **E**mission **T**omography
PG	**P**rompt **G**amma
PIN	***p***-type/ **i**ntrinsic/ ***n***-type diode
PMMA	**P**oly (**m**ethyl **m**eth**a**crylate) - acrylic glass
rel	**rel**ative
ROC	**R**ead**o**ut **C**hip
Si	**S**ilicon
sgl	**s**in**gl**e
SNR	**S**ignal to **N**oise **R**atio
SPECT	**S**ingle-**P**hoton **E**mission **C**omputed **T**omography
strg	**str**on**g**est
TCT	**T**ransient **C**urrent **T**echnique
Te	**Te**llurium
THM	**T**raveling **H**eater **M**ethod grwoth
VAM	**V**ertical **A**mpoule **M**ethod growth
VGF	**V**ertical **G**radient **F**reeze growth
yld	**y**ie**ld**
2D	Two-**d**imensional

List of Symbols

σ	neutron capture cross section	b
^{137}Cs	Caesium-137, main γ- emission at	661.657 keV
^{133}Ba	Barium-133, main γ- emissions at	276.398 keV
		302.8508 keV
		356.0129 keV
^{241}Am	Americium-241, main γ- emissions at	59.54 keV
Z	atomic number	
Z_{eff}	effective atomic number for compounds of more than one element	
BNC PG	BNC reaction prompt gamma at	477.59(5) keV
CdNC PG	CdNC reaction main prompt gamma at	558.46 keV

Chapter 1

Introduction

Imaging technologies are part of the most essential tools used in modern medicine. The first diagnostic devices were employed, within a year of Röntgen's description of X-rays in 1895, leading to the numerous applications of ionizing radiation that we have in medicine today.

Soon after the discovery of X-rays, reports of adverse effects such as hair loss or deep skin burns were reported. Nevertheless, it took until 1960 that the International Labour Organization (ILO) restricted workers from exposure to ionizing radiation in their Radiation Protection Convention (ILO, 1960). Partially based on this convention, the *ALARA* principle was developed. It states that the exposure to ionizing radiation (or other occupational health risks) should be *As Low As Reasonably Achievable*. This principle is one of the essential driving forces in the development of every new generation of ionizing radiation devices in medicine. In medical imaging the aim is to reduce the exposure for both the patient and the operator, while simultaneously increasing the image quality and diagnostic value. Through this effort we have come from photographic plates, via fluorescence screens to scintillator coupled photo diodes. Allowing us to quickly transfer the information obtained through ionizing radiation into digital signals that are used in medical applications. Nowadays, patient doses are only a fraction of the doses that were given with the first diagnostic images in 1886. Additionally, the image quality has dramatically improved. However, there is still room for further improvement.

The current imaging technology largely employed in medical imaging applications, is scintillator based (Bushberg et al., 2001; Nikl, 2006; Beckert et al., 2016; Pani et al., 2016). These

are energy-integrating detectors, thus energy of the absorbed radiation is not measured per single quantum, but integrated over a time interval. The next technological step is to employ direct conversion techniques, allowing the measurement of the absorbed radiation per single quantum. Detectors capable of this technique are called photon counting (PC) detectors in medical physics, as described by Hasegawa et al. (1991) for example. The development of these kinds of detectors requires substantial technological effort, but first prototypes have already been tested with positive results (Kalender et al., 2016; Pourmorteza et al., 2016).

The development of direct conversion detectors with photon counting capability will lead to profound improvements in medical (e.g. X-ray) imaging. By having access to the full detected spectrum, a single exposure can improve image contrast by revealing conventionally hidden differences in anatomic images (Roessl et al., 2007; Muenzel et al., 2016). Similarly, an analysis of the spectral composition of the recorded data can be used to efficiently separate different tissue types of similar density. This enables new diagnostic possibilities and increases accuracy (Schlomka et al., 2008; Wang et al., 2011).

However, the development of PC detectors for medical applications is heavily dependent on the detector material that is used. The basic functionality of such a detector is based on a diode structure, made from doped semiconductor materials (see Sections 3.1.2 and 3.1.3 for details). Although a number of semiconductor materials are known, only a small number qualify for the use as radiation detectors. Table A.1 in the Appendix lists the most promising candidates for the usage in medical applications, while basic physical principles and concepts for the usage of these candidates are provided in Section 3.1. The two most favored materials are Cadmium Telluride (CdTe) and Cadmium Zinc Telluride (CdZnTe/ CZT)[1]. These materials allow a good compromise between the requirements and the restrictions of ionizing radiation that is used in medicine. This is discussed in Section 3.1.3.

A remarkable example of the benefits of PC detection in medicine is presented in this thesis. It gives a glimpse of the

[1]Cadmium Telluride and Cadmium Zinc Telluride detectors are technologically similar to each other. All results of this work apply equally to both the CdTe and CdZnTe detector types.

possibilities that become available with the PC detector technology, but is not restricted to the given example.

1.1 Boron Neutron Capture Therapy

Boron Neutron Capture Therapy (BNCT) is a binary radiotherapy that has been under development for certain malignant tumors (Savolainen et al., 2013), since the 1930's. As in other radiotherapies, a lethal or accumulated lethal radiation dose is delivered to tumor cells, while the surrounding healthy tissues are exposed to non-lethal doses. For external radiotherapy this dose is delivered via high energy ($\sim$ MeV) photons, electrons or heavier particles, and radiation beams are generated outside the patient usually by an accelerating device. Brachytherapy is an example of a common internal radiation therapy. A sealed radiation source is usually placed (for example surgically) in or near the area of treatment. The lethal dose is then released to a localized volume, while tissues further away are not affected.
Neutron capture therapy (NCT) can be considered a third category. The lethal radiation dose is released locally by nuclear reactions that are occurring in a tumor seeking compound, if that compound is exposed to an external neutron radiation field (Locher, 1936). In boron neutron capture therapy (BNCT) this compound carries boron-10 (^{10}B) atoms that have a high neutron capture cross section of 3843 b at thermal energies of $E < 0.4$ eV (Chadwick et al., 2011).

BNCT has been evaluated in several clinical trials in the second half of the last century with good success rates (Mishima et al., 1989; Slatkin, 1991; Nakagawa et al., 1997). It may also be suited in combinations with traditional treatments such as chemotherapy, or surgery. The therapy can also be a last resort for patients that have exhausted all other therapeutic options. Newer clinical studies have demonstrated the safety and effectiveness of BNCT (Kankaanranta et al., 2012; Savolainen et al., 2013). In spite of the advantages of the therapy, three main issues remain to be solved before its general acceptance as an additional tool in radiation therapy (Wikipedia, 2017).

1. The development of more tumor-selective boron delivery agents for BNCT.

2. An accurate, real time dosimetry to better estimate the radiation doses delivered to the tumor and normal tissues.

3. The evaluation of recently constructed accelerator-based neutron sources as an alternative to nuclear reactors.

The first problem is mostly a pharmaceutical task and is not discussed further in this work. The last problem is currently under investigation as more accelerator based neutron facilities are being planned or come into operation (Kumada et al., 2011; Tanaka et al., 2011; Kreiner et al., 2014; Phoenix et al., 2015; Horiike et al., 2015; Biomedicum Helsinki Foundation, 2016). The application example of PC detectors of this work concentrates on the second issue, which requires the development of imaging and detector technologies. One possible method for the real time dosimetry is a similar approach to that applied in single photon emission computed tomography (SPECT). That is by imaging the prompt gammas (PG) resulting from the boron neutron capture (BNC) reaction and analyzing them for intensity and distribution. Several research groups have proposed BNCT specific SPECT methods, called BNCT-SPECT (Verbakel et al., 1997; Kobayashi et al., 2000; Rosenschöld et al., 2001; Minsky et al., 2009) with all aiming to provide the online dosimetric data, i.e. by counting and localizing the absolute number of BNC reactions within the patient.

However, a conclusion of the proposed BNCT-SPECT methods is that the signal background requires further reduction in order to identify the PG photons from the boron neutron capture reaction within the gamma and neutron induced gamma background spectrum (Kobayashi et al., 2000; Minsky et al., 2009). Thus, a poor signal to noise ratio (SNR) prevents active exploitation of the proposed BNCT-SPECT approaches. The logical course to increase the SNR, is to employ highly sensitive detectors with good energy resolution (hence PC detectors).

Common candidates are Germanium (Ge) detectors, which are counted among the most sensitive detectors with the best energy resolution available. However, their cooling and spatial requirements are not suited for clinical environments (Kobayashi et al., 2000; Savolainen et al., 2013). Section 3.1.3 outlines this circumstance. Furthermore, the lack of two dimensional (2D) detector arrays (e.g. detectors of 20 x 20 cm size, consisting of

hundreds or thousands of pixels) disqualifies Ge detectors for BNCT-SPECT.

The second detector type often evaluated for BNCT-SPECT are CdTe detectors. These detectors do not require excessive cooling and can be produced in 2D detector arrays. In the 2000s some groups started to investigate the usability of CdTe detectors in BNCT-SPECT (Kobayashi et al., 2000; Valda et al., 2005), with the conclusion that about 4% energy resolution is sufficient (Valda et al., 2005). Furthermore, appropriate neutron shielding and collimation techniques are required for its successful usage (Kobayashi et al., 2000). Back then, CdTe detectors did not fulfill all of these requirements. Devices with sufficient energy resolution were available, but at high prices and the non-availability of multi-pixel-spectrometers prohibited further investigations. Here, multi-pixel-spectrometers are referred to as 2D arrays capable of PC operation. These kind of detectors are required for SPECT like operations. Moreover, the shielding of the neutron background, which requires large filter structures made these detector types unfeasible for BNCT-SPECT.

Since then several technological advances have been made and new evaluations of the CdTe detector technology have been carried out. Improvements in the energy resolution (Kargar et al., 2010; Murata et al., 2014) and device sizes (Redus et al., 2006) were identified. This novel generation allows to efficiently detect and identify the PG photons from the BNC reaction (also called boron signal) in BNCT-SPECT. However, the SNR of the boron signal is still small compared to the large and always present gamma background and especially the neutron induced gamma background. This led to the author's hypothesis that the neutron induced gamma background could be classified as a second, dependent signal of the boron concentration and distribution in the tumor. Therefore, a modification of the BNCT-SPECT method was proposed in Publication I and is summarized in the following Section 1.2.

The ultimate aim of this work is to enable the accurate detection of ^{10}B distributions of a target (tumor) in a phantom (patient). This will enable a similar approach as published by Minsky et al. (2011), however by involving signals from both the BNC and cadmium neutron capture (CdNC) reactions. The presented approach allows tomographic reconstructions of the ^{10}B

distributions within a patient to become achievable. Furthermore, the determination of the radiation dose to tumor and healthy tissues as well as ascertaining the ^{10}B concentration in the tumor become feasible, if these calculations are based on the information obtained through both reaction types.

1.2 Modified BNCT-SPECT

The PG photons from the CdNC reaction (also called cadmium signal) can equally be utilized to determine the ^{10}B concentration and location of a tumor in BNCT-SPECT. These PG photons are related to the number of neutrons that pass a patient without being captured by the ^{10}B in the tumor. Hence, the overall number of detected neutrons (or for that matter PG photons from the CdNC reaction) are related to how many BNC reactions have taken place in the tumor. The more boron reactions have occurred, the larger the boron signal and the smaller the cadmium signal will be. Therefore, in the context of BNCT-SPECT, the number of neutrons that pass through the patient is a dependent function of the ^{10}B concentration.

Only a fraction of the neutrons from the epithermal neutrons beam are captured by the ^{10}B, whilst the largest part of the neutrons will pass through the patient. For this reason, the signal from the CdNC reaction is significantly larger than the signal from the BNC reaction. This improves the SNR of the cadmium signal compared to the boron signal.

Chapter 2

Aim of this Work

The aim of this work is to present possibilities to enhance current methods of medical imaging and radiation therapy through the use of PC detector technology. The usage of PC detectors in BNCT-SPECT is an example of how to enable the so far unsuccessful in-treatment detection of the PG photons from the boron neutron capture reaction. These PG photons can be used to determine the radiation dose to the tumor and healthy tissues, during the administration of the treatment. The specific aims of this work are:

1. The re-evaluation of a CdTe based spectrometer to detect the PG photons from the boron neutron capture reaction in BNCT-SPECT. Furthermore, the sensitivity and capability of the device to simultaneously detect PG photons from the BNC reaction and neutrons is to be tested (Publication I).

2. To verify the proposed modified method by obtaining agreement between experimental and simulated data, by means of evaluating nuclear data libraries and simulation output formats (Publication II).

3. To use the verified method to determine the position of boron-10 enriched targets, by experiment and simulations. Furthermore, to verify if the modified method could also be applied for boron-10 concentrations that are occurring during treatment (Publication III).

4. To enable data acquisition for the GaAs detector prototypes by reducing the electrical noise of the TCT setup, located at HIP premises (Publication IV). Furthermore, to

evaluate the GaAs detectors for their usability in medical applications.

5. To verify the operational functionality of pixel detector modules for the CMS pixel Phase I Upgrade -project. This task allows the evaluation of the usability of the CMS readout chip for applications in medical physics. The verification of the detector's functionality for the CMS project was achieved simultaneously (Publication V).

The results of Publication I led to the proposition for the modification of BNCT-SPECT. This had been discussed further in Publications I - III. The contribution to Publication V led to the production of the PC prototype at HIP. This prototype, described in Section 3.1.5, is ideally suited for its application in the next generation of medical imaging systems and the proposed modified method of BNCT-SPECT.

Chapter 3

Background and Methods

3.1 Radiation Detection

High energy radiation that is produced from nuclear decays, relaxations, cosmic radiation or in particle accelerators are detected by radiation detectors. Several kinds of detectors based on different physical effects, such as momentum, spin, charge and energy are used for specialized tasks of detection. The most common detection principles are based on ionization and scintillating effects, but other principles like Cherenkov-radiation, or simple defect induction are also used. This work is focused on radiation detection by ionization that occurs in solid state semiconductor detectors.

The outline of the physical processes of radiation detection and detectors is following the line of argumentation of Knoll (2010) and the Diploma thesis of the author (Winkler, 2017).

3.1.1 Principles of Radiation Detection

The basic interactions that occur in ionizing detectors are photo electrical- and Compton-effect, as well as pair production. Depending on the energy of the ionizing event, all three can occur simultaneously and are a function of the detection material. A typical interaction diagram is plotted for CdTe in Figure 3.1. The relative cross sections of the photo electrical effect (σ_{ph}), Compton-effect (σ_c) and pair production processes (σ_p) are a function of the energy of the absorbed photon (E_γ) and the atomic number (Z) of the absorbing material. The formulas of

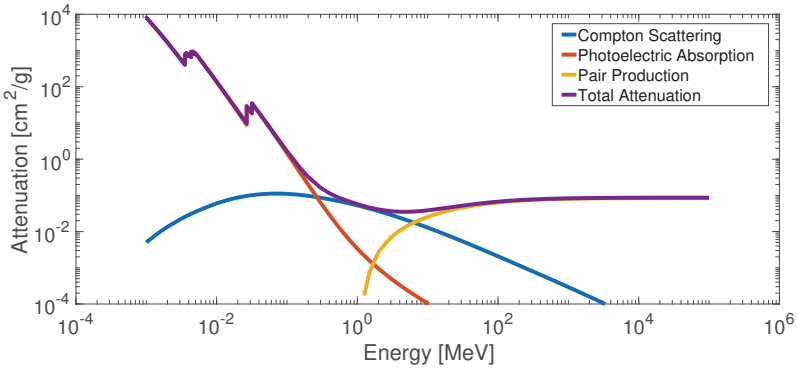

FIGURE 3.1: Attenuation of the three main interaction processes and the total attenuation in CdTe. Plotted with data from NIST, 2017.

Equation 3.1 approximate these relations (Knoll, 2010):

$$\sigma_{ph} \cong a_{ph} \cdot \frac{Z^n}{E_\gamma^{3.5}} \qquad \sigma_c \propto a_c \cdot Z \qquad \sigma_p \propto a_p \cdot Z^2 \tag{3.1}$$

with a_{ph}, a_c and a_p being constants for the photoelectric, Compton and pair production effect, respectively. From these relations one can see that photoelectric absorption is the major process of interaction in CdTe (Z_{eff}(CdTe) = 50 with $Z_{Cd} = 48$, $Z_{Te} = 52$) at photo energies that are relevant for medical imaging devices and the proposed modified method of BNCT-SPECT. These energies are < 600 keV[1].

3.1.2 Functionality of Semiconductor Detectors

Semiconductor radiation detectors are mainly based on *pn-* junctions, which are biased in one way or the other with an electrical potential (see Section 3.1.3 for variations with CdTe detectors). Due to this process, the area that is sensitive to radiation detection covers the semiconductor volume and in ideal cases the complete volume. The ionizing radiation creates charge carriers in the form of electron-hole pairs that travel within the electrical field to their respective electrodes. Consecutive read out electronics collect the charge carriers and process the information into a signal.

[1] Pair production does not occur for energies < 1022 keV.

Depletion Layer

A depletion layer forms after charge compensation at the intersection of a *p*- and *n*-type semiconductor. The resulting electrical field prevents further electrons and holes from entering the region. Any newly generated electron-hole pair (e.g. by ionizing radiation) will be pushed by the electric field out of the depletion region towards the collecting electrodes. This makes the depletion layer the active region where the process of radiation to signal conversion occurs.

The phrase *ionizing radiation* indicates the process of interest. A highly energetic particle (e.g. an X-ray photon) that passes through the depletion layer will lose its energy by the means of photoelectric absorption, Compton effect or pair production. These processes create electron-hole pairs along the path of the incident radiation. Further charge carrier pairs can be created by secondary events. However, the overall number of charges created is constant for a certain particle energy and material. This makes it possible to record energy spectra that refer to specific characteristics of an ionizing radiation event.

Energy Resolution

The energy needed to create one electron-hole pair in a semiconductor detector is of the order of a few electron volts (eVs). For CdTe and Gallium Arsenide (GaAs) these energies are 4.43 eV and 4.20 eV, respectively (Del Sordo et al., 2009); also listed in Table A.1. These low pair-creation energies enable the measurement of high energy resolution spectra with these materials, because even a low energetic ionizing event (a few keV) creates several thousand electron-hole pairs. Assuming complete collection of the created pairs, a count at a specific energy in the spectrum is recorded. Several counts at the same energy accumulate to peaks. Incident events of different energies create different numbers of electron-hole pairs and thus different peaks appear in a spectrum. These peaks can be used to identify the source or a nuclear reaction that has occurred.

The energy of the recorded event can vary dependent on further physical interactions such as Doppler broadening, or scattering effects. Additional, imperfections of the detector material can also change the number of electron-hole pairs that are created by the event. Finally, the readout electronics add further

distortions and noise to the recorded event. All these effects lead to a statistical distribution of the energy that is detected for incident events of a certain energy. If the energy of two adjunct peaks is closer than the average broadening of the detecting system, then these peaks can not be distinguished anymore. This leads to the definition of energy resolution. The higher the energy resolution of a detector system is, the closer two adjunct peaks can be, while still being distinguishable. The most common way to measure the energy resolution of radiation detectors is to evaluate the full width at half of the maximum center energy value (FWHM) of a peak. A guideline is that two peaks can still be distinguished if they are at least one value of FWHM at the measured energy apart.

Signal to Noise Ratio

The signal to noise ratio (SNR) is used to describe the efficiency of separating a signal from the background. It can be used to compare different devices and measurement setups. Its definition is the ratio of a signal divided by the noise of the signal. Within the scope of the results of this work, a *signal* is defined as the pulse peak height count number from either the BNC, or the CdNC reaction. Whilst *noise* is defined as the number of registered counts up to the baseline threshold, at the position of the signal. For example, the SNR of the BNC reaction of Figure 4.5 on page 37 (top part) at 45 mm is 1.4. This means that the boron signal is 40% larger than the noise at this position.

3.1.3 CdTe Detectors

Detectors made of CdTe have successfully been established as common room temperature radiation detectors and are already evaluated for clinical applications such as computed tomography (CT) and positron emission tomography (PET) scanners (Mikhaylova et al., 2013; Barber et al., 2015). Their energy gap of 1.44 eV is large enough to broadly prevent thermally generated charge carriers to be exited into the conduction band and thus reduce the thermal noise to acceptable levels. For comparison, detectors made of Ge have an energy gap of 0.67 eV, which allows significant thermal excitation of charge carriers into the conduction band at room temperatures. Therefore, Ge detectors

are cooled with liquid nitrogen (77 K), which reduces the thermal noise excitation to negligible levels. The larger energy gap of CdTe allows the omission of the bulky mechanics required by liquid nitrogen cooling systems. Therefore, more compact detector systems can be built.

The energy gap and the resulting leakage current of a detector are functions of the temperature. Varshni's approximation describes the energy gap of semiconductors as a function of temperature (T), (Equation 3.2 and Varshni, 1967):

$$E_{\text{gap}}(T) = E_{\text{gap}}(0) - \frac{\alpha T^2}{\beta + T} \tag{3.2}$$

where α is dE_g/dT and β in approximation the Debye temperature. $E_{gap}(0)$ and $E_{gap}(T)$ are the gaps energies at zero and the evaluation temperature. Figure 3.2 shows the energy gap of CdTe as a function of temperature leading to 1.44 eV at room temperature. The obtained energy gap value can then be used to calculate the leakage current I_{leak} of a semiconductor, Equation 3.3.

$$I_{\text{leak}}(T) \propto T^2 \cdot e^{-\frac{E_{\text{gap}}}{2k_B T}} \tag{3.3}$$

With k_B being the Boltzmann constant. Equation 3.3 illustrates the exponential dependence of the leakage current on the energy gap, and thus on the temperature. At 1.44 eV it is a relatively small value of approximately 10 nA (Figure 3.3). Conventional silicon (Si) based detectors and hadron irradiated Si detectors show currents of several µA, partially due to their smaller energy gap of 1.12 eV (Moll et al., 1999; Sze et al., 2006).

The higher effective atomic number of CdTe is the main reason for the substantially more effective absorption of higher energetic radiation compared to Si or Ge (see Equation 3.1). Furthermore, the electron-hole pair creation energy is small enough to allow for a good energy resolution. The crystal growth of compound semiconductors however, is not as simple as it is for elementary semiconductor materials, such as for instance Si. This results in a low production yield and a high price per detector (Su, 2015). Additionally, conventional doping as done for Si, to obtain *p*- or *n*-type materials is not possible with CdTe,

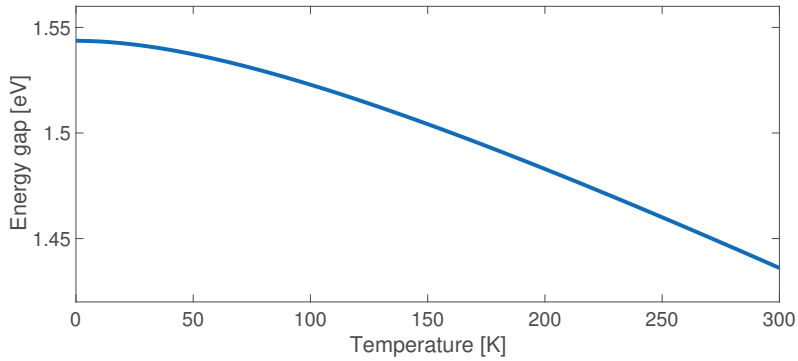

FIGURE 3.2: Energy gap of CdTe as a function of temperature, leading to a gap of 1.44 eV at room temperature (293 K).

due to the formation of opposite-charged defects or defect complexes and the low solubility of possible donor materials (Wei et al., 2001). Thus, *pn*-junctions are generally not available for CdTe. However, the diode effect and therefore, the depletion layer can be obtained with a blocking electrode. This is realized with a Schottky-diode type construction (Takahashi et al., 2002), allowing bias voltages up to a few kV and full depletion even for several millimeter thick devices. Alternatively, simple ohmic-type detectors are also available. The latter however, are less effective and are not used within the context of this work.

Suitable pieces of CdTe are usually cuboid volumes of a few millimeteres side length. The detector used in this work (Amptek X-123 CdTe, Amptek Inc., Bedford, MA, USA) employs a crystal of $3 \times 3 \times 1\,\mathrm{mm}^3$ volume that is large enough to absorb a substantial part of the radiation it is exposed to; assuming energies of $< 600\,\mathrm{keV}$ (Amptek Inc., 2016). In combination with suitable readout electronics, a clear identification of the radiation source is possible.

CdTe Material Quality and Processing

The reason for the comparably small sizes of CdTe detectors lies within the quality of the material. Unlike Si or Ge, the crystal growth process is substantially more complicated and requires precise control over numerous growth parameters (Li et al., 2016). Despite considerable efforts during the last decades,

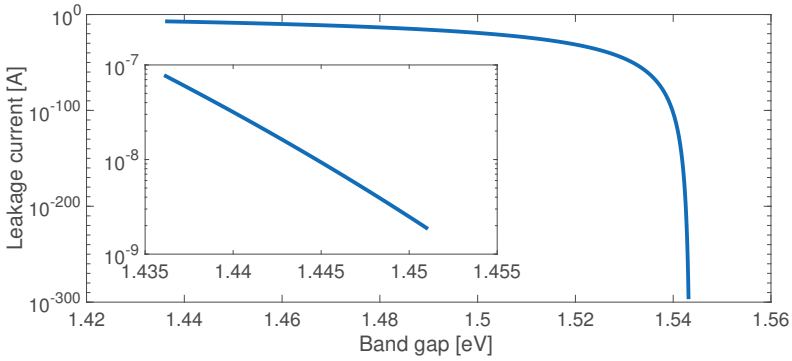

FIGURE 3.3: Leakage current of CdTe as a function of the energy gap with a closeup of smaller energies that are related to higher temperatures. The leakage current at room temperature (293 K) is typically some tens of nanoamperes.

only 2 inch diameter ingots are available (Jeong et al., 2014) that are containing a few large grains. Larger diameters still contain numerous smaller grains, which result in low single crystal production yields. This non-availability of large diameter ingots (and wafers) has a substantial impact on the detector production chain, as most devices and techniques of the semiconductor industry are designed for Si wafers of 6 inch diameter or larger and 300 µm thickness. Automated chip-scale processing, hence the processing of small cuboids of a few millimeters side length is largely impossible and thus requires manual handling. This increases the price further as well as the chance for errors. A slice of an CdTe ingot containing several larger grains is shown in Figure 3.4. In addition to the visible grains (Figure 3.4a), more defects that were revealed by infrared (IR) inspection are marked in Figure 3.4b. Several additional grain boundaries and crystallographic defects are visible, partially intersecting the volumes from which the detector are to be cut. Defects, such as grain boundaries or fractures inevitably lead to reduced detector performance. Therefore, intensive quality assurance is required for constant, detector performance (Szeles et al., 2006; Winkler, 2017). The mechanical properties of CdTe include fragility (Stahle et al., 1999) and low hardness (Zhang et al., 2008), which further complicate detector production processes. For example mask aligners that are used during the lithography

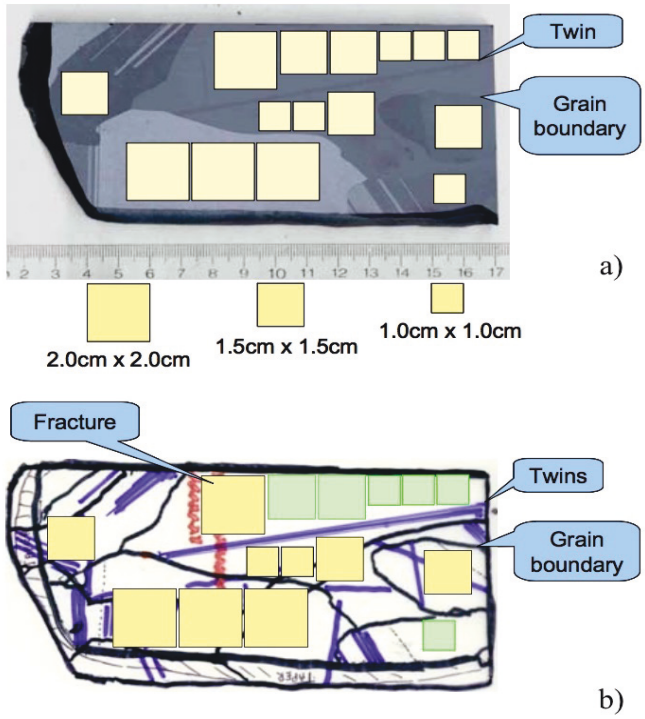

FIGURE 3.4: a) A CdTe ingot slice with several visible grains and marked volumes from which detectors are to be cut. b) The same slice under IR inspection, revealing additional defects that are intersecting the marked detector volumes. Adapted from (Szeles et al., 2006).

process, require certain contact pressure that can easily break a CdTe crystal. Furthermore, the fragility of CdTe leads also to reduced process temperatures of $<140\,^{\circ}\mathrm{C}$ (Riley et al., 2001) compared to Si processes. This temperature limit also has consequences on certain processes and chemicals that are commonly used during Si processing, because not all can be used for CdTe processing.

3.1.4 GaAs Detectors

Another semiconductor material that can be employed for room temperature radiation detectors is GaAs. This material is comprised of Gallium (Ga) and Arsenic (As) and maintains an energy gap of 1.43 eV and an electron-hole creation energy of 4.20 eV, see Table A.1 for more details. Both values are similar to

the properties of CdTe and a similar performance might be expected. However, the effective atomic number Z_{eff}(GaAs) = 32 (Z_{Ga} = 31, Z_{As} = 33) of GaAs is smaller than that of CdTe. This has direct impact on the relative cross sections of the photo electrical-, Compton-effect and pair production processes and thus, the effectiveness to convert ionizing radiation into charge carriers. The relations of Equation 3.1 allow an assessment of GaAs detectors for their usage in medical applications and for BNCT-SPECT. Therefore, an evaluation of the absorption coefficients for energies of < 600 keV is performed in Section 4.4.

The growth of the material is better understood than it is for CdTe and various growth techniques exist. For example, Liquid Encapsulated Czochralski (LEC), Chemical Vapor Deposition (CVD), Vertical Gradient Freeze (VGF) are commonly used (Scheel et al., 2009). In addition, sufficient control over the growth techniques can be achieved to allow the production of single crystal ingots of 2 inch diameters or larger. The mechanical properties of GaAs are similar to Si although at a lower temperature range (Yonenaga et al., 1987). Devices made of these semiconductors are also thermally stable (Sun et al., 2016). Therefore, many standard processes and instruments that are used for Si processing are compatible with GaAs semiconductors. Another advantage of GaAs over CdTe is that these semiconductors can be doped, hence *p*- and *n*-type materials are commercially available and thus various *pn*-junctions can be designed. The devices characterized for Publication IV were *p*-type/ intrinsic/ *n*-type (PIN) structured diodes, grown with a custom-made Chloride Vapor Phase Epitaxy (CVPE) method. The diodes had a diameter of 1.75 mm and a thickness of 110 - 130 µm.

3.1.5 Photon Counting Detectors

A spectrometer for radiation requires a large volume to efficiently stop the ionizing event. In addition, sophisticated readout electronics are necessary for high resolution spectroscopy. The latter usually contains only one input channel. Thus, spectrometers are usually made out of single planar electrodes (Knoll, 2010), which do not allow position sensitivity. Tracking and spatially resolved detectors, on the other hand, are simple counters of larger, but thin areas comprised of millions of

pixel or strip electrodes. The Si particle tracking detector system (Dominguez et al., 2012) of the Compact Muon Solenoid (CMS) experiment at the Large Hadron Collider (LHC) at CERN (Conseil Européen pour la Recherche Nucléaire, Meyrin, Switzerland), is a distinct example of a counting detector. However, no spectral identification is possible, as the ionizing event is usually not completely stopped within the detector. In addition, the subsequent readout chain is not designed to provide the spectral information, as the tracking detector is followed by calorimeters that measure the energy. The combination of spectrometric and position sensitivity is part of active research and is a crucial functionality for the proposed modification of the BNCT-SPECT method of this work. Devices in astro- and particle physics, that are capable of recording spatial resolved spectra, are referred to as pixelated spectrometers (Alvarez et al., 2011). In medical physics these devices are called photon counting detectors, although describing essentially the same device (Shikhaliev et al., 2011; Yu et al., 2015; Kalender et al., 2016). The discussion of technical details of these combined instruments goes beyond the scope of this work and the reader is kindly referred to the dedicated literature; for example Wilson et al. (2013), Macias-Montero et al. (2015), Muenzel et al. (2016), and Symons et al. (2017). The terms *detector* and *spectrometer* are used interchangeably in this work, however this may not apply outside of this work.

A prototype of a photon counting detector based on CdTe that was build at the detector laboratory of the Helsinki Institute of Physics (HIP, Helsinki, Finland) and is presented in Figure 3.5. A readout chip (ROC) designed for the CMS pixel phase I upgrade Publication V at the LHC was flip chip bonded to a CdTe crystal. The extensive measurements required to characterize the ROC and its functionality for the CMS pixel phase I upgrade Publication V revealed that the chip is in principle compatible with CdTe detectors and allows operation in PC mode.

3.2 Monte Carlo Simulations

Monte Carlo (MC) simulations are widely used to help to understand and analyze nuclear processes. In medical physics, particularly in radiotherapy, the MC simulations are used to calculate

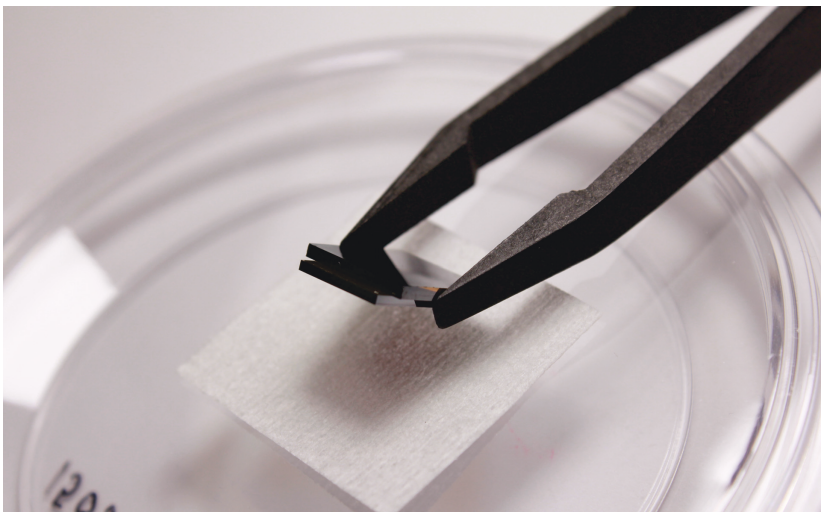

FIGURE 3.5: Prototype of a PC capable detector for the use in e.g. medical applications. The CMS ROC is on the bottom and the CdTe element on the top. The active detector material has a thickness of 1 mm.

the patient dose and to simulate the detector response, e.g. expected counts. In MC and in particular MCNP (Monte Carlo N-Particle code, Monte Carlo Team, 2003a) simulations rely heavily on input libraries that contain data for the nuclear processes and their products that are to be simulated. Several research groups have specialized in maintaining and extending these libraries (Chadwick et al., 2011; Koning et al., 2012; Shibata et al., 2012), but discrepancies between measured and simulated data are found regularly (El Kanawati et al., 2011; Chadwick et al., 2011, Publication II). Furthermore, depending on the software version used, not all nuclear process can be simulated simultaneously. This leads to inconsistent results for mixed radiation fields, in which the products of one type of radiation influence the results of another type. The mixed neutron and photon radiation field of BNCT is a particular example for that. The use of correct data libraries and results calculations are essential for MC simulations in medical physics and especially for the proposed modified BNCT-SPECT method. MCNP5 version 1.4 is used in this work (Monte Carlo Team, 2005).

3.2.1 Tallies F8 and F4

Depending on the problem, several calculation options can be chosen in MCNP. These are called tallies and are indicated with the letter *F* in MCNP. The F8 tally for example allows to simulate the pulse height spectrum measured by the detector. Furthermore, patient doses can be calculated with the energy deposition version (*F8) of this tally (DeMarco et al., 2002; Ye et al., 2004). The F4 tally on the other hand, provides the total track length flux of particles (including photons) of a cell (Monte Carlo Team, 2003a). The *cell*, is in the context of MCNP and this work, the volume of the object, for which the flux is simulated. The F8 tally is most useful for radiation therapy as the dose deposited to a medium can be calculated, although with possibly less accuracy than with comparable codes (Koivunoro et al., 2012). However, the F8 tally does not allow the calculation of mixed radiation fields with neutrons. For BNCT-SPECT simulations this means that the pulse height spectrum of a combined electron, photon and neutron field can not be calculated directly. An error will be returned if simulations of the F8 tally of a neutron field is attempted (Monte Carlo Team, 2003b). The correct calculation of pulse height spectra for mixed radiation fields with neutrons is however essential for the proposed modified BNCT-SPECT method (Section 1.2). The F4 tally does allow this combination, but is not designed to provide pulse height spectra of detectors. Nonetheless, it is still possible to simulate a pulse height spectrum of CdTe with the F4 tally. The required procedures are presented in Section 4.2 and Publication II.

3.3 Experimental Setups Used in this Work

3.3.1 BNCT-SPECT

The experimental data of the Publications I - III of this work, were obtained with the epithermal neutron beam at the TRIGA Mark II (FiR 1) reactor in Espoo, Finland (Auterinen et al., 2001). In each case a cylindrical plastic phantom made of polymethylmethacrylate (PMMA, length 240 mm, diameter 200 mm) was used to represent a patient's head (see Figures 3.6 and 3.7). For each setup, different inserts were placed along the central axis (also referred to as the depth axis) of the phantom. First,

plain PMMA inserts representing the patient before the boron agent has been given. Second, some of these inserts were replaced with boronated polyethylene (PE, 3-wt% B, which is $\approx 2100\,\mu g/g$ of ^{10}B) cylinders (length 19 mm, diameter 30 mm), representing a patient's tumor enriched with ^{10}B, Figure 3.8. These PE cylinders were placed at a depth of 19 - 57 mm from the phantom's surface, which is a typical working distance for epithermal neutron beams (Monshizadeh et al., 2015). During experiments using the third setup, the PE cylinders were replaced by a PE phial (length 108 mm, diameter 27 mm) containing boric acid water with 400 $\mu g/g$ ^{10}B concentration. The phial was placed to start from the surface of the phantom. The three setups will be referred to as *Phantom*, *Tumor* and *B-water* in this work. An experimental configuration similar to the one presented in Figure 3.6 was used for all setups.

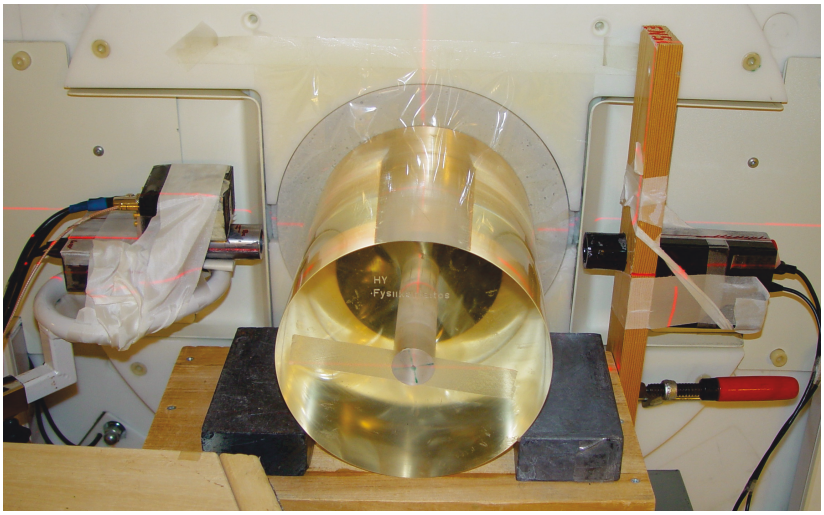

FIGURE 3.6: General experimental setup used for Publications I - III. The detector is located inside the silver lead shielding on the left that also acts as a collimator. For the first experiments, the detector was kept stationary and was moved along the depth axis of the phantom for later experiments.

The detector used in all experiments is an Amptek X-123 CdTe spectrometer (Amptek Inc., 2016). For Publications I, the detector was placed at a fixed position and distance from the phantom, as illustrated in Figure 3.6. For Publication III the detector was moved in several steps parallel along the phantoms

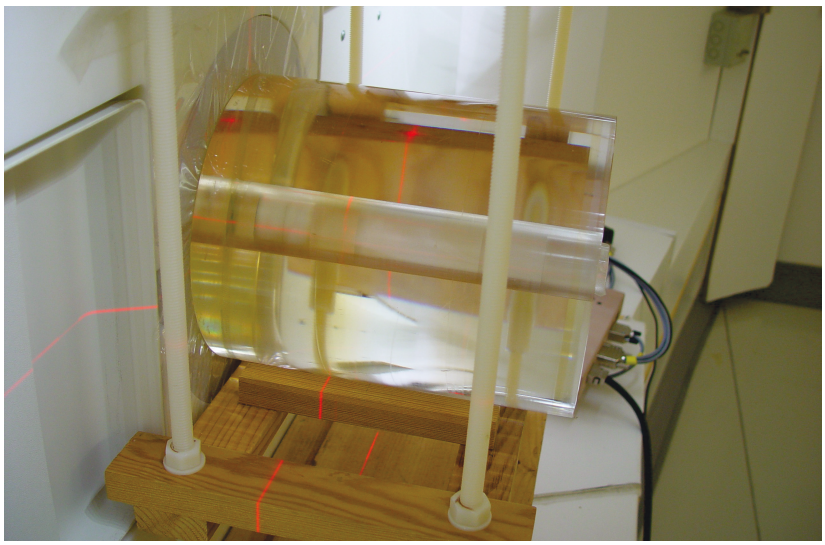

FIGURE 3.7: Close up of the phantom with boronated target inserts. The (white) PE targets used for the Tumor setup are visible on the left hand side of the phantom.

depth axis. The detector itself was shielded with a 6 mm lead housing encasing the whole device and acting as a collimator with a length of 22 mm. Further, a linear energy calibration was performed using ^{133}Ba and ^{137}Cs isotopes. This resulted in resolutions (FWHM) of 2.56 keV at 356 keV and 5.99 keV at 662 keV, respectively. The detector efficiency at 500 keV is approximately 5.6% (Amptek Inc., 2002).

3.3.2 Transient Current Technique Test Setup for GaAs Diodes

A custom design Transient Current Technique (TCT) setup was used for Publication IV. The TCT is used for measuring the effective concentrations of charge carriers in *pn*-junction detectors made of various materials (Eremin et al., 1996). The TCT setup at HIP contains measurement specific, low-noise preamplifiers, bias-Ts[2] as well as a red and an IR laser. The later are used to create charge carries in the semiconductors under test. All components are located inside a light-tight metal enclosure. After

[2]Bias-Ts are devices that allow to combine (separate) signals from (into) their components of direct- and alternating current.

FIGURE 3.8: Boronated PE (3-wt% B) targets used for the Tumor setup.

preamplification, signal amplitudes of the order of mV are expected for the GaAs diodes. These are significantly smaller than the signals of Si diodes. This is partially due to the higher resistivity of GaAs (see Table A.1). Significant efforts were undertaken to reduce the electrical noise of the system, in order to enable the acquisition of the data that were presented in Publication IV.

3.3.3 CMS Pixel Phase I Module Testing Setup

The setup used for Publication V is a standard probe station that is available at the clean room facilities of HIP. A custom made, multichannel probe card was used to allow temporary electrical connection to the CMS ROC `PSI46DIG` (Dominguez et al., 2012); see Figure 3.9. Once a connection was established, a series of electrical tests were run to determine the functionality of the ROC. Besides the large amount of ROCs that were tested, substantial effort was put into noise reduction of the testing system. Both have led to a deeper understanding of the ROCs functionality and its possible usage with CdTe detectors.

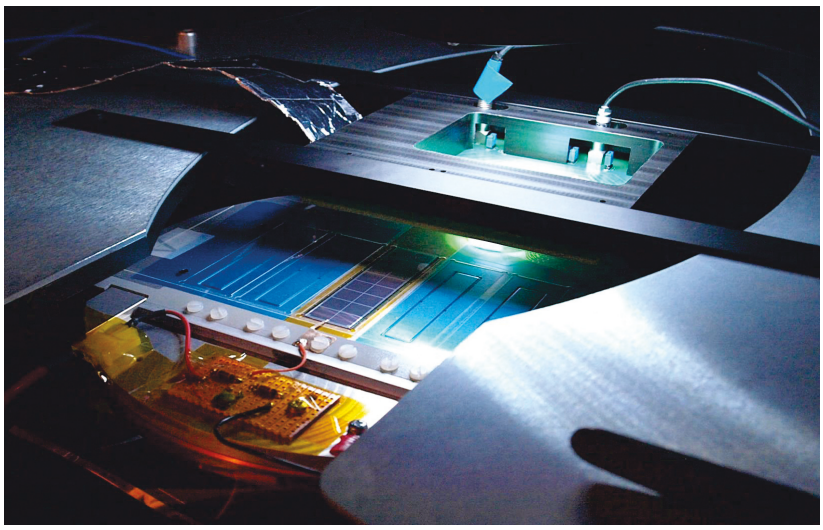

FIGURE 3.9: A CMS pixel Phase I Upgrade module (middle) under test in the HIP probe station.

3.4 Tools Used in this Work

This section briefly describes the principles and relations required to follow this work. All these principles are well-known and are discussed in depth by various sources in the literature.

3.4.1 Nuclear Reactions Required for the Modified BNCT-SPECT Method

The nuclear reaction on which BNCT-SPECT is based on, is the BNC reaction ^{10}B(n,α)^{7}Li. A thermalized neutron ($E_n \leq 25$ meV) is captured by a ^{10}B atom, followed by the release of an α particle and an excited ^{7}Li atom. This occurs with 94% probability. The relaxation process of the ^{7}Li atom takes place quickly ($\sim 10^{-13}$ s) under the release of a PG photon of the energy of 477.59 keV (IAEA, 2007; Knoll, 2010). The nuclear capture process ends with a 6% probability directly in the ground state of the ^{7}Li atom. The neutron capture cross section (σ [b]) of ^{10}B is with 3843 b comparably large at thermal energies (Chadwick et al., 2011), while most of the other isotopes possess a neutron capture cross section in the scale of 10 b or less.

Equally important for this work is the nuclear reaction that occurs if a thermalized neutron is captured by a ^{113}Cd atom of the detector. This transmutes the ^{113}Cd atom into an excited ^{114}Cd atom, which relaxes under the release of a PG photon or conversion electrons of 558.46 keV, within $\sim 10^{-12}$ s (Casten et al., 1992). The PG photon is released with a probability of 74.4% (NNDC et al., 2017). This is the CdNC reaction ^{113}Cd(n,γ)^{114}Cd. The probability that a thermal neutron is captured is very large (20609 b) at thermal energies (Koning et al., 2012). A CdTe detector made of natural Cd and Te possesses about 6.11% ^{113}Cd in its volume. The large neutron capture cross section and detector thicknesses of 1 mm or larger allow a near total absorption of all thermal neutrons reaching the detector. The PG photons released from the capture process are captured with approximately 66% probability in the same detector volume. Due to the production and capture of the PG photons in the same medium and the short travel distances, a virtually undistorted signal (e.g. by Doppler-broadening) can be observed. This leads to sharp and clear peaks in the spectrum that can easily be identified with known PG emissions from the CdNC process.

3.4.2 Data Analysis

All raw data obtained from the CdTe spectrometer, such as presented in Figure 4.1, have been filtered with a moving average filter to compensate for noise and statistical fluctuation. Additionally, a baseline correction is performed to compensate the lower attenuation efficiency of higher energy photons. Finally, besides Figure 4.1, all spectra are plotted within an energy window of 440 - 590 keV, which is the window of interest for the proposed modified method of BNCT-SPECT. The measurement error of the spectrometer is based on an estimation of the detector response to the calibration sources. A small error is observed for larger count numbers (>50). This error increases linearly for peaks with count numbers close to the background level (<10).

The uncertainty of the simulations is the statistical relative error (with confidence level of 1 standard deviation) provided by the MCNP results and is $\lesssim 5\%$ for the BNC and approximately 1% for the CdNC reaction. Higher accuracy would have

required the extension of the simulation time beyond reasonable length. Furthermore, all simulated results have also been smeared with the energy resolution measured for the CdTe detector and were plotted in the same energy windows of interest as the measured data.

Chapter 4

Results and Discussion

4.1 Proof of Concept of the Modified BNCT-SPECT Method

In this section, the usability of modern CdTe spectrometers for BNCT-SPECT and a proof of concept for the proposed method is presented. The evaluation of modern CdTe spectrometers in gamma and neutron radiation fields is done with a focus on the evaluation of adequacy of the energy resolution and sensitivity of the detector for BNCT-SPECT. In addition, the ability to detect the signals from both BNC and CdNC reactions is studied. The results of these discussions are presented briefly here, a more detailed analysis can be reviewed in Publication I.

4.1.1 Sensitivity and Energy Resolution

The raw spectrum obtained from the CdTe spectrometer, with the Phantom Setup and in the neutron field of the FiR1, is presented in Figure 4.1. The presence of distinct peaks is an evident sign of a sufficient energy resolution for BNCT-SPECT. The most important peaks are marked (from left to right) in Figure 4.1 and in Table 4.1. The energy resolution at the largest peak (#5) is 4% (22 keV), which is equal to resolution required by Valda et al. (2005) and below the minimum of 33 keV that was estimated by Murata et al. (2014). The difference between the centroids of peaks #5 and 6 is with 19.62 keV the smallest difference between all the peaks in the area of interest. It is with $\approx$4% also within the requirement for the energy resolution set by Valda et al. (2005). In addition, peak #5 and 6 can clearly be distinguished from each other in Figure 4.1. Therefore, CdTe spectrometers of the present technological level possess a high

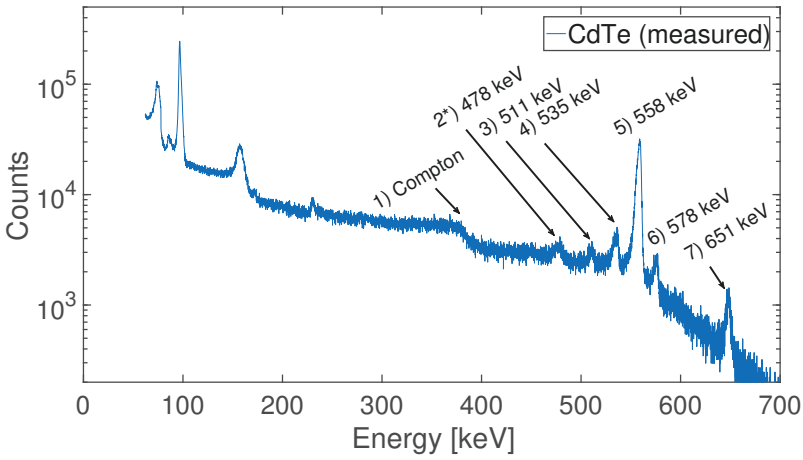

FIGURE 4.1: Raw spectrum of the Phantom setup recorded with an epithermal neutron flux of $1.07 \cdot 10^7$ n/cm^{2}s for 15 min. The important peaks for this work are marked with their energies.

enough energy resolution for their usage in BNCT-SPECT. Furthermore, the presence of the discrete peaks # 2*, 4 - 7 proves that it is possible to define neutrons as a signal and not as background with this detector. Hence, it can be used for simultaneous gamma and neutron detection.

The spectrum of Figure 4.1 has been obtained with 1% reactor power, which relates to a epithermal neutron flux of $1.07 \cdot 10^7$ n/cm^{2}s, at an accumulation time of 15 minutes. This flux produced a well pronounced spectrum with sufficient statistics to clearly identify the peaks and their energy. Shorter accumulation time (approximately $1/10$ length), or lower reactor power are still likely to produce sufficiently large peaks. Hence, the spectrometer is sensitive enough for the desired purpose.

4.1.2 Signals from Boron Neutron Capture and Cadmium Neutron Capture Reactions

The signal from the BNC reaction is the most essential information for BNCT-SPECT, while the signal from the CdNC reaction is additionally important for the proposed modification of the method. Both signals can be measured if a reference situation without boron is available. The raw spectrum of Figure 4.1 that

TABLE 4.1: Peaks, corresponding energies and relative production yields (rel. yld.) marked in the spectrum of Figure 4.1.

Peak #	Energy [keV]	Description
1	380.00	Compton edge
2	477.59	BNC PG (main emis. 94% rel. yld.)
2*	477.60	CdNC PG (minor emis. $\leq$ 1% rel. yld.)
3	511.00	Annihilation peak
4	535.26	Cd, Te sgl. escape (strg. 5% rel. yld.)
5	558.46	CdNC PG (main emis. 100% rel. yld.)
6	578.08	CdNC PG (minor emis. 6% rel. yld.)
7	651.26	CdNC PG (minor emis. 19% rel yld.)

has been taken with the Phantom setup can be considered as such a reference situation. During the actual therapy, this information could be obtained by *illuminating* (low neutron flux of $\leq 10^7$ n/ cm^{2}s) the patient for some time, before the boron agent boronophenylalanine (BPA) is administered. The accumulated additional patient dose at these fluxes is <1% and thus, can be considered negligible. Spectra that are obtained after the boron agent has been given contain the desired information. The difference between both spectra reveals the signal that is produced by the ^{10}B. This difference can be used to calculate the ^{10}B concentration and location within the phantom (patient).

The Tumor setup is obtained by placing a boronated target (2100 µg/g of ^{10}B) into the phantom. This represents the administration of the boron agent to the patient. The spectrum obtained from this setup is compared to the Phantom setup and is plotted in Figure 4.2. The difference between both spectra is emphasized with a shaded area. The peak from the CdNC reaction is decreased by approximately 2200 counts and the peak from the BNC reaction is increased by about 900 counts, if ^{10}B is present in the phantom. The peak details are listed in Table 4.2 for comparison. As described in Section 1.2, the signal from the CdNC is larger than the BNC signal, as the number of neutrons that pass through the patient is substantially larger than the number of neutrons that are captured by the ^{10}B. This is the reason why the CdNC signal can be detected easier and

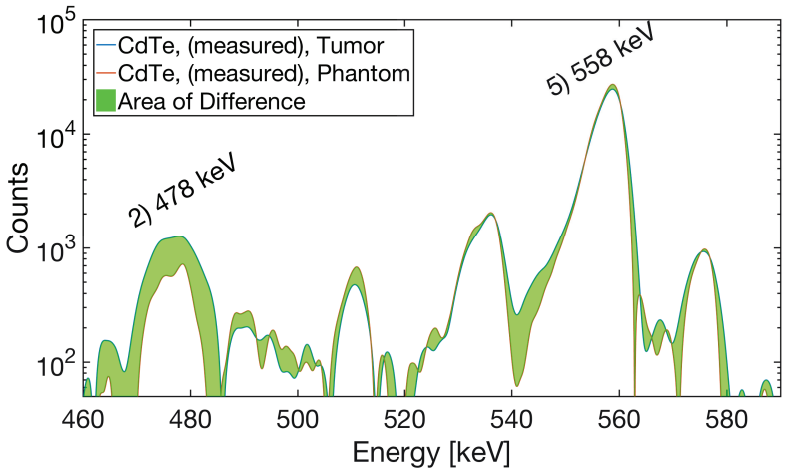

FIGURE 4.2: Comparison spectrum of the Phantom and Tumor setups. The difference (shaded area) at the BNC and CdNC reaction peaks is clearly visible, if ^{10}B is present in the phantom.

has a larger SNR with less statistical fluctuation. Therefore, the measurement of the CdNC signal is more accurate than the measurement of the BNC signal. This opens the possibility for more accurate patient dose calculations. Additionally, the CdNC signal from the Phantom setup is larger than the CdNC signal from the Tumor setup, which proves that less neutrons are scattered towards the detector if ^{10}B is present in the phantom. The opposite situation is observed for the BNC reaction peak, which increases, if ^{10}B is present in the phantom.

The presence of a peak at the BNC reaction energy, even though ^{10}B is not present in the Phantom setup, is no contradiction. The peak #2*, at the energy of approximately 480 keV, shown in Figure 4.2, originates from several minor PG emissions of the CdNC reaction (NNDC et al., 2017). The strongest emission is at 477.60 keV, which is almost exactly at the same location as the PG peak from the BNC reaction itself (477.59 keV). The intensities of these minor CdNC emissions are $\leq 1\%$ compared to the main PG emission at 558.46 keV, but are significant ($\approx 50\%$) compared to the number of detected BNC reaction events. These additional PG emissions are, however, always present if a CdTe

TABLE 4.2: Comparison of peak heights (in counts), energy resolutions (ΔE in keV) and peak height differences (Δ in counts) of the BNC and CdNC reaction peaks, presented in the spectrum of Figure 4.2.

	Phantom	**Tumor**
BNC	876	1780
ΔE_{BNC}	3.10 ± 0.04	0.90 ± 0.02
CdNC	22148	19944
ΔE_{CdNC}	13.10 ± 0.17	10.50 ± 0.20
Δ_{BNC}		+ 904
Δ_{CdNC}		- 2204

spectrometer is used in a neutron field. Therefore, these emissions are added towards the systematic background of the proposed method.

The sufficient energy resolution, the sensitivity and the ability to detect both BNC and CdNC reaction peaks demonstrate the feasibility of the proposed approach for BNCT-SPECT, because it is possible to detect signals from both gamma and neutron radiation fields. The difference between the two setups is clearly visible and the sensitivity of the detector for low neutron fluxes (compared to the therapy) is sufficiently high for the proposed modified method for BNCT-SPECT to be formulated.

4.2 Simulations and Method Specific Properties

This section focuses on discussion of the simulations that are required to verify the data measured with the CdTe detector and explains how to obtain such simulations. The discussion is extended to some specific properties of the modified BNCT-SPECT method.

4.2.1 Simulations

A pulse height response spectrum of the Tumor setup has been simulated (Figure 4.3) in order to obtain a spectrum similar to the one that was measured. The standard MCNP nuclear data library *ENDL92* (Los Alamos National Laboratory, 2004) and

the tally F8 were used. The PG peak from the BNC reaction at 478 keV, which is most important for BNCT SPECT, is present in all spectra, but underestimated compared to the measured peak. In addition, the PG peaks from the CdNC reaction are completely missing from the simulated spectra. Yet, these were measured simultaneously with the rest of the gamma spectrum, as the indicated by the graph *CdTe, (measured)* of Figure 4.3. The reason for the missing PG peaks from the CdNC reaction is that MCNP5 in version 1.4 is not simulating the energy deposition of neutrons with the F8 tally. In addition, simultaneous simulations of the photo and neutron spectra are not possible. Hence, the F8 tally cannot reproduce the PG photons that occur as a result of neutron capture within the detector.

Since the pulse height spectrum of CdTe detectors in a neutron field can not be simulated correctly, a detour via tally F4 is investigated. The F4 tally is defined as the flux over the detec-

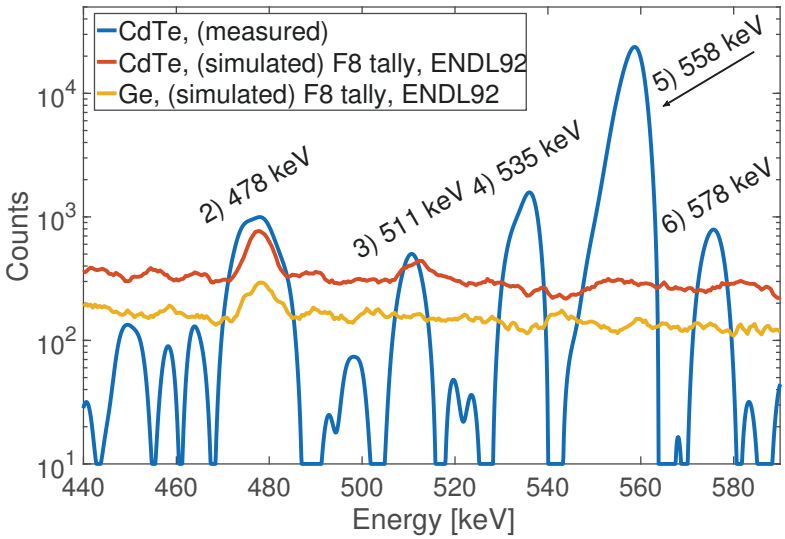

FIGURE 4.3: Example of simulated PG spectra of CdTe and Ge detectors for the Tumor setup, simulated with the ENDL92 library and tally F8. The peaks from the CdNC reaction (#4 - 6) are completely missing and the BNC peak (#2) is underestimated, compared to the measured spectrum. The peak numbers refer to Table 4.1.

tor volume. This is in principle the number of net photons that

will enter the detectors volume, sorted by energy. The flux includes the PG photons produced from neutrons in the detector volume, hence covers simultaneous photon and neutron spectra. This also introduces some drawbacks. For example, the F4 tally may also include photons that leave the detector volume before being detected. Furthermore, a simulated detector will convert every electron-hole pair that is created by a photon into a readable signal, whilst this process is less efficient in a real detector. The simulations can not account for crystallographic imperfections in the detector, electrode materials and software settings of the readout electronics, which all reduce the number of detected events by real detectors. These drawbacks result in simulated peak heights that are approximately 11 - 13 times larger than the peaks of the measured spectra. However, these larger peak heights can be corrected by normalizing e.g. the PG peak from the CdNC reaction of the simulation to the same peak of the measured data. This peak is chosen, because it is the largest in the region of interest (440 - 590 keV). Consequently, it has the smallest statistical uncertainty. Nevertheless, any other peak can also be used for this normalization.

To obtain successful simulations of spectra recorded with CdTe detectors in a neutron field, one also has to choose an appropriate nuclear data library. Particular attention should be put into the completeness and correctness of the gamma production tables for the isotopes simulated. MCNP uses these tables to generate gamma photons and their probability as results of the nuclear processes that were simulated. If a correct nuclear data library — like TENDL-2008-ACE (Koning et al., 2008; OECD, 2017) — is used and a normalization applied as described above, then simulated spectra such as presented in Figure 4.4 can be obtained. A detailed discussion of this topic can be found in Publication II. The marked peaks correspond to peak numbers 2 - 6 from Table 4.1. The escape peaks (with 5%, 1.5%, 1.5% and 0.4% yield, respectively) were not simulated, as this functionality is not included in the F4 tally. Nevertheless, the simulations based on the tally F4 clearly represent the measured data better than the simulations based on the F8 tally (Figure 4.3). Thus, a method to simulate a measured spectrum of CdTe detectors in a neutron field has been identified.

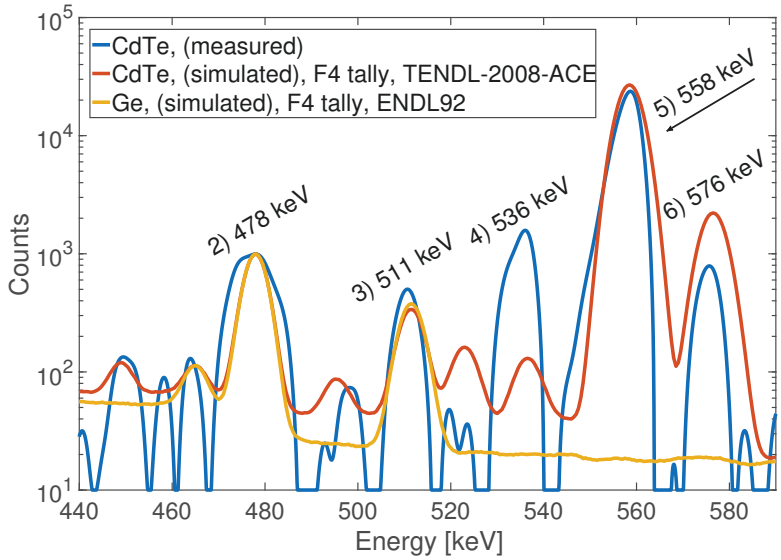

FIGURE 4.4: Simulated PG spectrum of the same configuration as in Figure 4.3, but with tally F4 and the TENDL-2008-ACE library. Besides peak #4, all the relevant peaks are present (see the text for a discussion). Peak numbers refer to Table 4.1.

Simulation of the Measured Data

Spectra that allow a comparison between Phantom and Tumor setups can be obtained, if the method above is applied. The resulting simulated spectra are compared to the measured spectra in Figure A.1a on page 54. This figure shows that the graphs of the simulations represent the measured situation adequately. The BNC reaction peak is larger if ^{10}B is present in the phantom (Tumor setup) and simultaneously the CdNC reaction peak is smaller. On the other hand, if ^{10}B is not present (Phantom setup), then the peak height of the BNC reaction peak is decreased, while simultaneously the peak of the CdNC reaction is increased. Figures A.1b and A.1c are closeups of the BNC and CdNC reaction peaks, respectively.

The spectra presented in Figure A.1a - c show that it is possible to simulate measured spectra appropriately, as they would

occur in the proposed modified BNCT-SPECT method. Therefore, verification of treatment data and more important prediction of patient doses become possible.

4.2.2 Method Specific Properties

In order to measure spectra from CdTe detectors, as presented e.g. in Figures 4.1 – 4.4, certain requirements for the detector size must be fulfilled. These spectra can only be obtained if the detector volume and especially its thickness are small compared to typical Ge detectors (>50 cm^3). A CdTe cube of 1 cm side length (1 cm^3), will already produce a spectrum with less energy resolution and a substantially larger annihilation peak, compared to the spectra presented in Figures 4.2 – 4.4. Photons of higher energy, like the 2.2 MeV photons from the $^1H(n,\gamma)^2D$ reaction will be captured with significant efficiency, which adds more peaks to the spectrum. Annihilation and escape events induced by these photons can create additional smaller peaks that might interfere with peaks of interests (e.g. the BNC reactions peak). Furthermore, it can be more challenging to design read out and bias electronics for the detector. Last, the raw material price of cubes of CdTe of 1 cm length is considerably larger than for square detectors of 1 cm length and only 1 mm thickness. In terms of these disadvantages, thicknesses of 1 - 5 mm are a good compromise.

Thin detectors on the other hand, have the advantage of being cheaper and easier to handle for the readout electronics. Moreover, these detectors are nearly transparent for high energy photons such as the ones from the $^1H(n,\gamma)^2D$ reaction. This allows lighter device structures, as less shielding is required. Additionally, the detectors life time is prolonged due to less induced radiation damage. Thin detectors (approximately 1 mm) also reduce the energy range of the spectrum to a maximum of about 800 keV, which is sufficient for the energy range of interest (400 - 600 keV) of the proposed modified BNCT-SPECT method.

4.3 Usability for Treatment Conditions

The previous section discussed the topic of data verification by means of simulations. Based on these, the usability of the proposed modification for BNCT-SPECT is discussed in this section.

A potential method to localize a boronated target, utilizing either of the two nuclear reactions is presented together with further simulations. In addition, an evaluation of the SNR and the dependency of the signals to the ^{10}B concentrations are made. All the figures of this section that consist of 2 subfigures show the results from the BNC reaction on the top half of the figure, while the results of the CdNC reaction are presented on bottom half of the figure.

4.3.1 Scan Along the Depth Axis of the Phantom

The first verification of the usability has been done by measuring spectra at 4 different positions along the depth axis of the phantom. These 4 positions are approximating a line detector of 4 pixels. The results of the measurements and corresponding simulations are presented in Figure 4.5.

The difference between the setups (Phantom and Tumor) of the BNC reaction peak at step 1 (depth = 45 mm) is 11 counts (Figure 4.5, top). The BNC reaction peaks from both setups can clearly be distinguished from each other, which indicates that the target is present in this area. This difference decreases with increasing distance along the phantom depth. Outside the target area (depth $\geq$ 95 mm) a count drop following an inverse square function (fitted graphs of Figure 4.5) is measured. Using the fitted graphs, a decrease of 21 counts for the Tumor Setup is measured, compared to the position at 45 mm, whilst the counts of the (fitted) Phantom Setup are reduced by 17 counts at this position. The signal from the boronated target therefore has a difference of 4 counts. The measurement at 95 mm depth of the Phantom Setup has higher counts than expected and it can not be completely ruled out that this measurement point is an outliner due to unknown processes in the experiment. Therefore, the values of the fitted graphs have been used for the calculations of the signal difference at this location. For the CdNC reaction a similar, but inverted situation can be observed (bottom of Figure 4.5). The CdNC reaction peak height of the Phantom setup is larger than the same peak of the Tumor setup, as more neutrons reach the detector. A difference between both setups can be observed at step 1. For steps 2 - 4, this difference gradually decreases, suggesting that no target is present at these steps. The decrease in counts is less abrupt as they were for

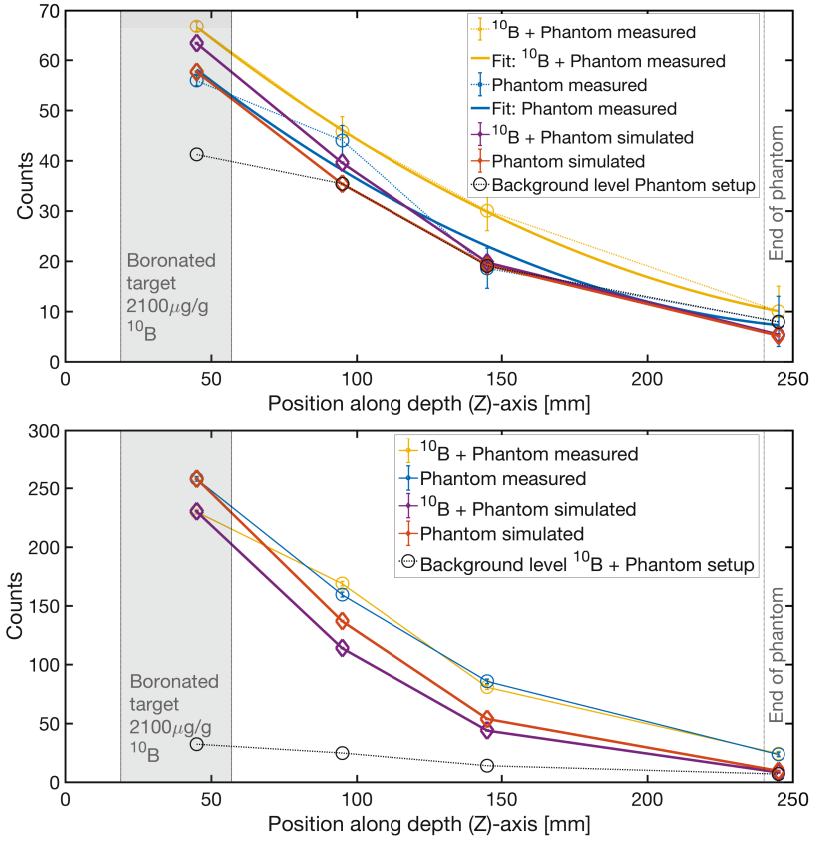

FIGURE 4.5: PG peak heights of the BNC- (top) and CdNC- (bottom) reactions peaks for different positions along the depth axis of the phantom.

the PG photons from the BNC reaction, because the neutrons are not affected by the lead collimator of the detector. Apart from the outliner at depth = 95 mm, the simulations of these experiments support our findings. The count difference between both setups is also at step 1 the largest for the simulations. This applies equally for both reaction types. The SNR of the CdNC reaction is at the target position approximately 7.1, while it is only 1.4 for the BNC reaction. In addition, the SNR drops down to approximately unity (1) at positions 2 - 4 for the BNC reaction, whilst it is always larger than 1 for the CdNC reaction. This further supports the assumption that the SNR of the CdNC reaction is superior to that of the BNC reaction, if the CdNC

reaction is used as a signal. A detailed discussion of all aspects of Figure 4.5 can be found in Publication III.

4.3.2 Virtual Line Detector

Clear signal differences in the spectrum can be measured with only 4 locations along the depth axis of the phantom, however higher spatial resolution is required to locate the target. For this reason, a line detector consisting of 42 pixels separated by lead collimators was simulated for the Phantom and Tumor setups. The resulting spectra are presented in Figure 4.6. The location of the boronated target and the end of the phantom are indicated in the Figure, as well as the measured data that was described in the section above. The first data point of the 4 step scan is approximately located at pixel number 8, when counting from the beginning of the depth axis. The differences in counts between the Phantom and Tumor setups are clearly visible for both reaction types. Especially, the signal from the BNC reaction benefits from the inter-pixel collimators, as the area of elevated counts from the Tumor Setup is placed in the area of the actual target location. This already allows a coarse localization between 10 - 70 mm along the depth axis of the phantom. The SNRs of both Phantom and Tumor Setups of the BNC reaction reach the noise level (SNR = 1) at about 100 mm depth. The CdNC reaction reaches this level at a depth value of 200 mm. A clear separation between the counts of the Phantom and Tumor Setup of the CdNC reaction is also visible. However, a coarse localization is not easily possible due to the gradual decrease of the count difference of the Phantom and Tumor setup.

Target Localization

A localization of the target from a data set such as the one of Figure 4.6 can be performed by applying the algorithm below. Whereas, the algorithm of Equation 4.1 is a naïve example to indicate the similar treatment of the photons and neutrons by the algorithm. The fields of inverse mathematics (e.g. Mueller et al., 2012) and statistical signal processing (e.g. Särkkä, 2013) offer more sophisticated methods. Essentially, the algorithm L takes the second derivative of the absolute count difference, that

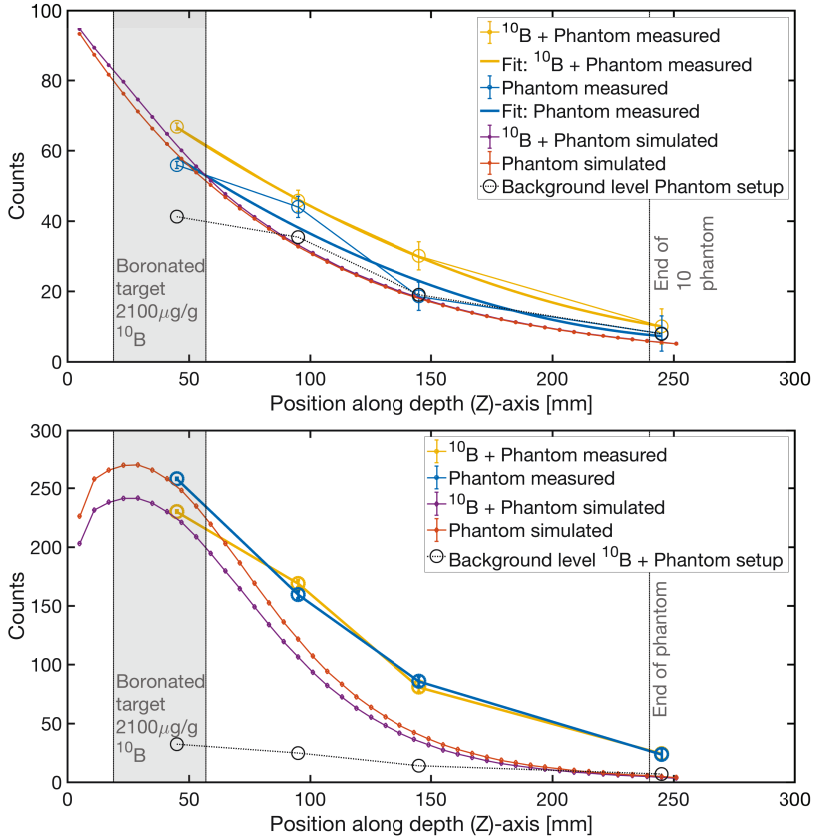

FIGURE 4.6: PG peak heights of the BNC- (top) and CdNC (bottom) reactions measured by a simulated line detector with 42 segments of $3 \times 3 \times 1\,\text{mm}^3$ along the depth axis of the phantom. Each pixel was simulated with a 22 mm collimator and 3 mm of lead spacing.

is obtained when subtracting the results from the Tumor and Phantom Setups.

$$L(n) = \frac{d^2}{d_{counts}^2} \Big(|\text{Phantom} - \text{Tumor}| \Big) \tag{4.1}$$

Here n indicates the *n-th* simulated detector element (pixel) along the line detector. The target identification is performed by choosing the detector element located before the global minimum of L as the starting point of the target. While the detector element before the global maximum of L identifies the end of the

target. The results from this calculation are shown in Table 4.3 (top) on page 45 and in Figure 4.7. The target location is marked with a shaded gray area and the detector elements that indicate the beginning and end of the target are marked with a bold line. The relative uncertainty of L is dependent on the detector element being evaluated and is the sum of the corresponding uncertainties obtained from the simulations of the Phantom and Tumour Setups. The uncertainties are plotted as errorbars in Figure 4.7. The largest error is 1.9% and $<0.3\%$ for the BNC and CdNC reactions, respectively. The spatial uncertainty of L is dominated by the pixel size, a value of ± 1.5 mm is assumed for all pixels. The algorithm L allows the localization of the target at $(20\text{-}56 \pm 1.5)$ mm depth of the phantom based on the BNC reaction (asterisk markers) and at $(8\text{-}116 \pm 1.5)$ mm depth based on the CdNC reaction (diamond markers). Especially, the results based on the BNC reaction are in good agreement with the real location of the target, which was simulated at (19 - 57) mm depth. The localization based on the CdNC reaction is less accurate, however, possible even with this naïve approach. Thus,

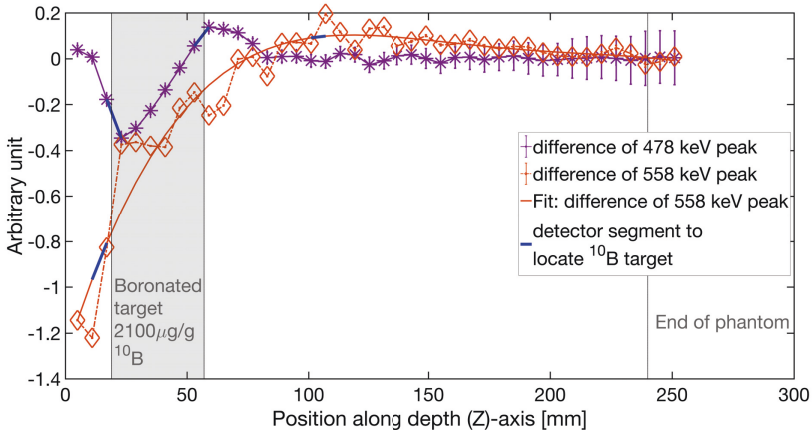

FIGURE 4.7: Visualization of the localization function L as described in Section 4.3.2. For the BNC reaction (asterisk markers), the target location coincidences with the detector element before the global minimum and maximum of L. For the CdNC reaction (diamond markers), the localization is less accurate.

an approximate target localization, based solely on the neutrons

that pass through the phantom (patient) is feasible. The accuracy can be increased by taking neutron scatter effects into consideration when evaluating the CdNC signal (Hassanein et al., 2005). Even though the presented simple target localization that is based on the CdNC reaction does not provide additional accuracy compared to the localization based on the BNC reaction, it can still be used for the purpose of validation. A combination of both localization results might also improve the accuracy. Additionally, a redundant validation source will become increasingly important at the ^{10}B concentration levels that are actually used during BNCT. The results presented up to this point were obtained with a high ^{10}B concentration target of 2100 µg/g, while treatment levels are substantially lower (approximately $1/40$), as will be discussed next.

4.3.3 Lower Concentrations of ^{10}B

Further reactor tests and simulations were performed, to answer the question if lower ^{10}B concentrations can still be detected with modern CdTe spectrometers. A boric acid phial containing 400 µg/g of ^{10}B was employed as a target. The corresponding results are presented in Figure 4.8 and are comparable to the 4 step scan along the depth axis obtained with the high concentration target.

After correction of the simulated data, results close to the expected and measured values were obtained (details in Publication III). The concentration of 400 µg/g ^{10}B in the B-water phial is 81% smaller than the ^{10}B concentration in the PE target (2100 µg/g) of the Tumor setup. Therefore, a BNC reaction signal from the B-water setups that is 81% smaller than the signal from the Tumor setup is expected, simulated and measured. In case of the BNC reaction with the boronated target, this relates to a net signal of 2 counts, at 58 counts. For the CdNC reaction the 81% signal reduction results in an increase of 22 counts, at 253 counts. Both compared to the signals that are obtained with the high boron concentration target that is used in the Tumor Setup. Both the measured and simulated data match these expectations well. For the BNC and CdNC reaction 59 counts and 253 counts are obtained. The SNR of the BNC and CdNC reactions at 95 mm depth (length of the boric acid phial) is 1.3 and

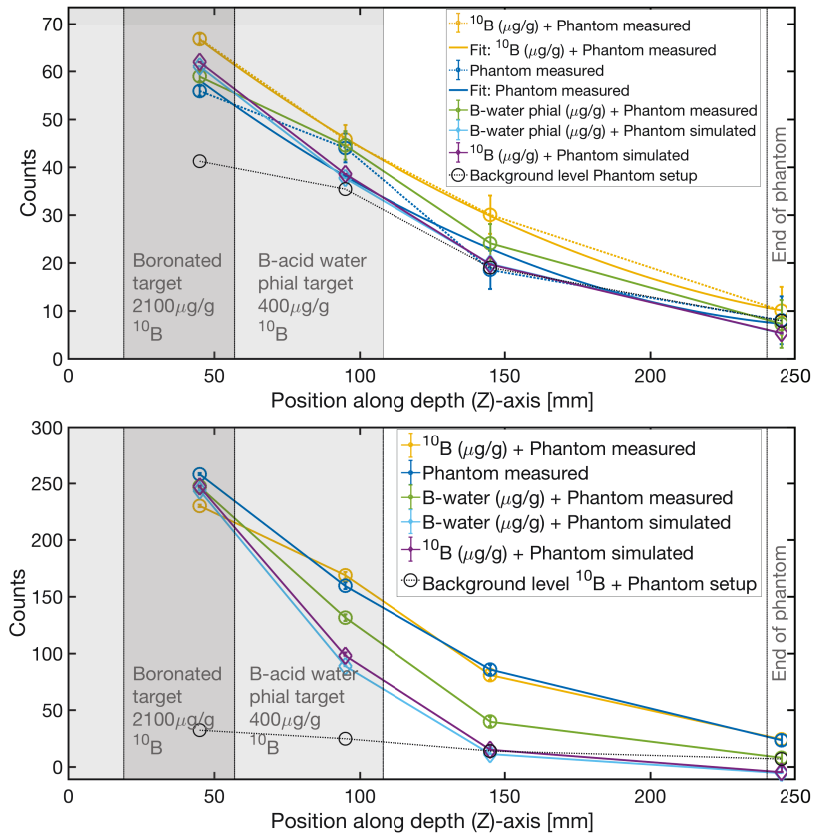

FIGURE 4.8: PG peak heights of the BNC- (top) and CdNC (bottom) reactions for different positions along the depth axis of the phantom. The counts from the B-water phial (400 µg/g ^{10}B) are located between the Tumor (2100 µg/g ^{10}B) and Phantom setups.

4.6, respectively. Additional accuracy can be obtained by applying further corrections as described in Publication III. Supplementary discussions of the remaining measurement positions of the B-water setup are also done in Publication III. Either-way, 400 µg/g of ^{10}B lie well within the range of sensitivity of the detector and the signal strength can be predicted accurately.

The typical real treatment concentration of ^{10}B however are still smaller in BNCT. Concentrations up to about 50 µg/g have been reported (Coderre et al., 1998). In order to determine if these realistic low concentrations can still be detected with modern CdTe spectrometers, further simulations of the B-water

setup were performed. The results of these simulations suggest that ^{10}B concentrations of $< 5\,\mu g/g$ can still be detected with the proposed approach. The details of this discussion can also be found in Publication III.

4.3.4 Simulations with Realistic Boron Target Concentrations and Boron Background in the Phantom

The experiment of Section 4.3.2 was repeated, to investigate if it is possible to detect realistic concentrations of ^{10}B with the line detector. A target concentration of $52.5\,\mu g/g$ ^{10}B and additional of $15\,\mu g/g$ ^{10}B, homogeneously distributed in the phantom were simulated. This represents a boron concentrations of 3.5:1 for tumor and healthy tissue as described by Kankaanranta et al. (2012). The through L determined difference (B-water phial mi-

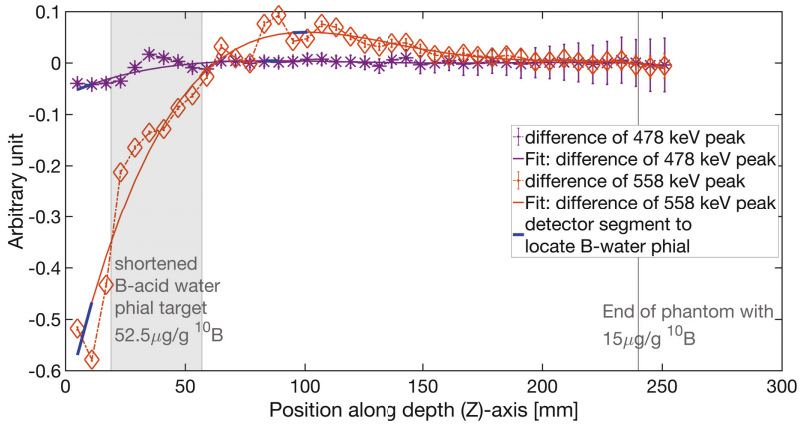

FIGURE 4.9: Simulated PG peak height differences from the BNC- (asterisk markers) and CdNC- (diamond markers) reactions for $52.5\,\mu g/g$ ^{10}B in the B-water target and $15\,\mu g/g$ ^{10}B in the phantom, representing a tumor to tissue boron ratio of 3.5:1. Localization is still possible for both reactions.

nus pure water target) is presented in Figure 4.9 and is with < 1 and with $< 0.1\%$ uncertainty, small for both reaction types. Nevertheless, a difference can still be identified. A localization of the target was attempted based on algorithm L of Section 4.3.2. The

detector segments that identify the beginning and end of the target are indicated. A localization based on the BNC reaction succeeds, despite the small difference of 0.05 provided by L. The target is located at a calculated phantom depth of $(8\text{ - }86 \pm 1.5)$ mm, while the real target location is modeled from (19 - 57) mm, i.e., the shaded gray area of Figure 4.9. This is a lower accuracy compared to the high concentration target and is expected due to the small signal difference. The flattened incline of the L function in Figure 4.9 represents this lower signal difference. It also shows that the differences of the BNC reaction are close to the detection limit as the global maximum of L is not significantly larger than the rest of the graph. Therefore, an additional target localization and/ or confirmation is desirable. The difference from the CdNC reaction on the other hand is larger (0.7, $< 0.1\%$ uncertainty), which also allows a successful localization based on this reaction type. The beginning of the target is calculated to be at (8 ± 1.5) mm and the end at (98 ± 1.5) mm. All results are listed in Table 4.3 (bottom). Again the CdNC results are less accurate than the location obtained with the BNC reaction, as the neutrons are not affected by the lead collimator of the detector. However, the minimum and maximum of the L function are more distinct, which shows that the difference of the CdNC signal is larger. Thus, it is easier to detect. Dedicated neutron localization algorithms are required for better results.

These results show that a potential target localization by using the BNC or the CdNC signal alone is also possible at realistic ^{10}B concentration levels in tumor and the surrounding healthy tissues (^{10}B concentration ratio of tumor to healthy tissue of 3.5:1), if modern CdTe spectrometers are used. The results also show that the information of the neutrons that pass through the patient can be used to locate, or confirm the location of a tumor. This is especially important under treatment conditions and at smaller SNRs, because the localization based on the BNC reaction of the realistic target is significantly less accurate than the localization obtained with the high concentration target that was used in Section 4.3.2.

TABLE 4.3: Calculated localization of a 2100µg/ g ^{10}B target inside a phantom (top) and for a boric acid in water target of 52.5µg/ g ^{10}B inside a phantom with 15µg/ g ^{10}B concentration (bottom). The localization is calculated with the algorithm 4.1. All numbers are in mm.

	Beginning between pixels located at	Average location	End between pixels located at	Average location
BNC (2100µg/g ^{10}B)	17 – 23	20 ± 1.5	53 – 59	56 ± 1.5
CdNC (2100µg/g ^{10}B)	5 – 11	8 ± 1.5	113 – 119	116 ± 1.5
BNC (52.5µg/g ^{10}B)	5 – 11	8 ± 1.5	83 – 89	86 ± 1.5
CdNC (52.5µg/g ^{10}B)	5 – 11	8 ± 1.5	95 – 101	98 ± 1.5
Actual target location		19		57

4.4 Testing of the GaAs diodes

In order to measure the TCT signal from the GaAs diodes, the corresponding setup, required improvements to reduce the electrical noise interference. Several sources of noise were identified for this setup. First, a large opening acting as a cable feed through. Second, the preamplifier was not on the same electrical ground level as the metal enclosure. Last, the signal cable connecting the GaAs diode and the preamplifier had a length of about 40 cm. Especially, the last issue is of importance as Ohmic losses and electrical interference (cable acting as an antenna) can reduce the signal amplitude below the noise level. These sources of noise were eliminated by the closing the Faraday cage with conductive tape, electrically connecting the chassis of the preamplifier to the metal Faraday cage and reducing the detector – preamplifier cable length to 10 cm. After elimination of these noise sources, the data presented in Publication IV were collected.

Several GaAs diodes and detectors were produced into radiation detectors for Publication IV. These can also be operated in PC mode, assuming appropriate readout electronics are used (Wu et al., 2014). However, due to the lower absorption efficiency of GaAs compared to CdTe, larger detector thicknesses are required for effective usage in medical applications. In order to achieve a similar absorption efficiency as 1 mm CdTe at 100 keV X-ray energy, a GaAs crystal of 15 mm thickness is required. The produced prototypes on the other hand, were only 110 and 130 µm thick. Thus, the resulting detector's efficiency is too low for use in most medical applications including BNCT-SPECT. Larger thicknesses require further optimization of the custom-made CVPE method, in order to reduce intrinsic stresses and wafer bowing (Wu et al., 2015). Hence, a more matured detector production process is required. The application in the soft X-ray range (≤ 33 keV) as used in mammography, might however still be feasible. For these applications, GaAs could be a viable solution, as production costs for large panel detectors (typical mammography imaging cassettes are $24 \times 30\,\mathrm{cm}^2$) are likely to be lower than for CdTe detectors.

4.5 Testing of the CMS Pixel Phase I Upgrade Readout Chip

HIP constructed 250 of the 672 sensor modules required for the pixel Phase I Upgrade of the CMS tracker at the LHC. Each module consists of 16 ROCs, with each one required to pass dedicated electrical and noise tests. These were described in the corresponding technical design report (Dominguez et al., 2012). A probe-station with a custom made probe card is required to establish temporary electrical connection to the ROCs and to conduct the module tests. It is essential that Both the probe station and -card are operated in a low noise environment. Thus, extensive efforts were undertaken to identify the sources of the electrical noise and their reduction. Such noise sources are system specific and therefore require individual solutions for every device and location.

Two large sources of noise were identified. First, an incomplete Faraday cage of the probe-station and second, electrical noise induced by surrounding devices through the power grid.

These sources were eliminated by reinforcing and adding additional electrical connections to each component of the probestation housing and thus closing the Farraday cage. The second noise source was eliminated by adding an isolation transformer to the power line of the measurement devices.

The CMS module testing was performed after successful reduction of the noise. More than 1000 ROCs have been tested for their functionality. These tests revealed the additional PC operation mode that was intended as a debug function during the design phase of the ROC. This mode was tested by irradiating one CMS pixel Phase I Upgrade module with an ^{241}Am source. The obtained spectrum is presented in Figure 4.10.

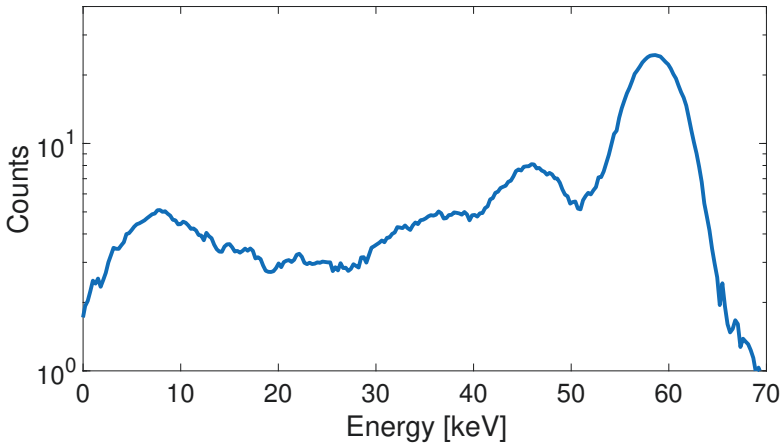

FIGURE 4.10: An ^{241}Am spectrum recorded with a CMS pixel Phase I Upgrade module. The main photopeak at 59.54 keV is indicated. The detector is a 300 µm Si detector, flip chip bonded to a CMS ROC.

The main photopeak of the ^{241}Am source is dominating the spectrum at 59.54 keV. The energy resolution is approximately 17%, which is only a fraction of values achieved by standard Si-PIN detectors (Amptek Inc., 2017). A direct comparison however, should be made with caution, because standard Si-PIN diodes are designed as cylindrical volumes similar to Ge detectors and not as 300 µm thin tiles. Thus, only a qualitative comparison is possible.

Nevertheless, testing the CMS pixel Phase I Upgrade modules revealed that the employed ROC is a suitable candidate for

PC operation in medical applications. In combinations with a CdTe detecting element, these ROC are a suitable option for a 2D detector array that can be used in BNCT-SPECT. Therefore, HIP started to investigate if PC detectors based on CdTe and CMS ROCs can be produced. The processes required for the production of electrodes on the CdTe crystals and to flip chip bond these to the ROCs, were developed by HIP and Advacam Oy at Micronova (Espoo, Finland). The prototype presented in Figure 3.5 on page 19 is a result of these efforts. The evaluation of this prototype has been set for future work.

Chapter 5

Conclusions and Future Work

The first major task of this work was to test the suitability of a modern, PC CdTe spectrometer for BNCT. It was found that the detector is highly sensitive and produces good signal statistics, even at neutron fluxes as low as 1% of the values that are used during the treatment. Furthermore, the energy resolution of the detector is good enough to allow the identification of the photo peaks relevant for the proposed modified method of BNCT-SPECT. Additionally, it was verified that both the BNC and CdNC reactions are dependent on the presence of ^{10}B in the phantom (Publication I). These results led to the formulation of the proposed modification of the BNCT-SPECT (Section 1.2).

After the principle of the proposed method had been shown, the topic of verification by means of simulations was addressed (Publication II). It was found that simulations of the pulse height response spectra (tally F8 in MCNP code) for CdTe detectors in neutron fields did not reproduce the measured data. An investigation of this topic revealed that the PG peaks from the CdNC reaction are missing in standard nuclear libraries. A secondary cause was found to be a restriction of the employed version of MCNP5 version 1.4, which does not allow the simulation of response spectra, if photon and neutrons fields are simulated simultaneously. This situation was resolved by using a combination of an alternative output tally (F4 instead of F8), a specific nuclear library (TENDL-2008-ACE; Koning et al., 2008) and normalization of the received results to measured data. This combination allowed verifications of the measured data that were presented in Publication I.

After both, the proof of the concept and the numerical verification of the proposed modification to BNCT-SPECT were achieved, an evaluation of a closer-to-treatment situation was performed. The primary task was to assess if the boronated target of a high ^{10}B concentration (2100 µg/g) can be localized in the cylindrical phantom. A 4-point scan along the central axis of a phantom was performed, coarsely localizing the target with both reaction types. Based on these results, a line detector consisting of 42 CdTe pixels was simulated and a target localization was performed using the signal from either reaction type. The most accurate results were received with the information of the BNC reaction, whilst the CdNC reaction results were less accurate, but still allowed successful localization. Nevertheless, the signal from the BNC reaction suffered from low SNR values, just as previous BNCT-SPECT attempts had suffered. The signal from the CdNC reaction on the other hand, showed up to five times larger SNR values, which allowed better distinction from the background.

Further experiments confirmed that the modern CdTe sectrometer is capable of detecting signals from a target of approximately 80% lower ^{10}B concentration. Supplementary simulations suggest that realistic target treatment concentrations of $\approx$50 µg/g ^{10}B can also be detected. Therefore, additional simulations were performed to investigate if the signals of a realistic treatment concentration are still detectable. These concentrations were 52.5 µg/g ^{10}B in the target and an additional 15 µg/g of ^{10}B homogeneously distributed in the phantom. A localization of the target was possible for both reaction types. However, the location obtained through the BNC reaction was substantially less accurate so that confirmation through the CdNC reaction is required (Publication III).

The results suggest that improvements in target localization can be achieved if the detector area is increased, which allows the detection of more events from the BNC reaction. Additionally, neutron collimators and dedicated localization algorithms for each reaction type are likely to contribute further improvements. A 2D detector array will also allow image reconstruction in three dimensions.

The reduction of electrical noise for the TCT setup at HIP was successfully achieved, allowing the measurement of small signal amplitudes. The feasibility of GaAs detector for medical

applications was discussed with the result that these materials might be an option for soft X-ray applications, assuming thicker detectors can be produced.

Finally, a measurement setup to test the detector modules for the CMS pixel Phase I Upgrade -project was installed and tested at the clean room facilities of HIP. The test setup was thoroughly adjusted to reduce the electrical noise background and allow high precision measurements. Over a thousand CMS ROCs have been tested and their functionality was evaluated. This allowed a deeper understanding of the chip and its possible usage as a PC detector in medical applications. A prototype of a CdTe element on a CMS ROC has been build by the CMS group of HIP. An evaluation of the prototype and its performance is set for future studies.

Research Conclusion

The main goal of this thesis was to investigate novel detector technologies for medical applications. The next step in medical imaging and therapy, is the employment of PC detectors. These kinds of detectors allow the acquisition of spectra of the applied radiation for each pixel of the detector. Whilst the majority of currently used detectors record the intensity only. The spectral information can be used for numerous applications and diagnostic improvements. A distinct example that benefits from the usage of PC detectors was presented for BNCT. This therapy lacks an accurate method to determine the ^{10}B concentration and distribution within the patient and during the treatment. A SPECT like approach, has been favored to determine the ^{10}B concentration and is called BNCT-SPECT. This approach employs the PG signal of the BNC reaction, but fails because of the low SNR ratio of this signal. This is due to the small number of PGs from the BNC reaction, as compared to the overall number of background photons and the number of neutron induced photons from the epithermal neutron beam.

A method has been proposed (Publication I and Section 1.2) to improve BNCT-SPECT by employing PC detectors based on CdTe. In addition, to the high sensitivity for the PGs from the BNC reaction, these detectors are also sensitive to the PGs from the CdNC reaction, which occurs within the detector itself. The

signal from the CdNC reaction is, like the signal from the BNC reaction, dependant on the amount of ^{10}B present in the patient. The CdNC signal however, possesses a larger SNR value and is therefore easier to detect in BNCT-SPECT. Both the BNC and CdNC signals can then be used for dose determination and localization efforts.

It is the PC ability of the detector however, which allows this modification to the therapy, because only through the PC operation, the distinction of both reaction types and the background from one another, become possible.

Recommendation for Future Research

For the future, it is suggested that further verification of the proposed modified BNCT-SPECT method should be performed. Mainly, the experimental evaluation of the target localization based on both reaction types is required for further developments. This can be achieved by repeating the experiments as described in Publication III and employing a line detector, or a 2D detector array comprised of PC CdTe detectors. Such an array will also enable tomographic image reconstruction. In cooperation with the development of dedicated localization algorithms, real time target localization and dose calculations become possible in BNCT-SPECT.

Unfortunately, such a detector array did not exist at the time of writing this thesis. Therefore, efforts should be invested to further the development of CdTe based PC detector arrays. The CMS group at the detector laboratory of HIP has started these efforts and the evaluation of the first prototype is expected to contribute not only to BNCT, but to the entire field of radiation detection in medicine.

Appendix A

Additional Figures and Tables

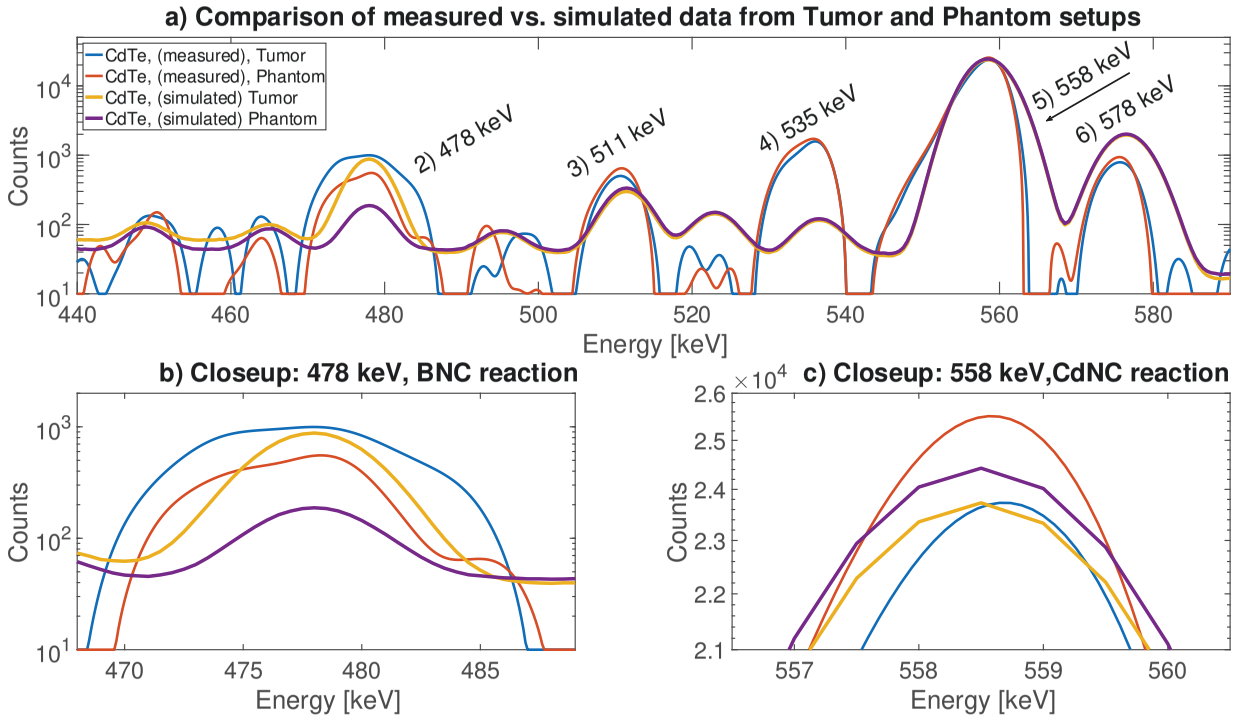

FIGURE A.1: a) Comparison of simulated and measured data of the Tumor and Phantom setups, recorded for Publication I. The BNC and CdNC peaks are simulated in the correct order of magnitude. Closeup of the BNC and CdNC peaks in Figures b) and c), respectively. A count difference between the Phantom and Tumor Setups is present for both measured and simulated data.

TABLE A.1: Physical properties of the semiconductors and compound semiconductors that qualify for radiation detectors in medicine at T = 25 °C. Adapted from Del Sordo et al. (2009).

Material	**Si**	**Ge**	**GaAs**	**CdTe**	**$Cd_{0.9}Zn_{0.1}Te$**	**HGI_2**	**TlBr**
Crystal structure	Cubic	Cubic	Cubic (ZB)	Cubic (ZB)	Cubic (ZB)	Tetragonal	Cubic (CsCl)
Growth method *	C	C	CVD	THM	HPB,THM	VAM	BM
Atomic number	14	32	31, 33	48, 52	48, 30, 52	80, 53	81, 35
Density (g/cm^3)	2.33	5.33	5.32	5.85	5.78	6.40	7.56
Energy gap (eV)	1.12	0.67	1.43	1.44	1.57	2.13	2.68
Pair creation energy (eV)	3.62	2.96	4.20	4.43	4.60	4.20	6.50
Resistivity (Ω cm)	10^4	50	10^7	10^9	10^{10}	10^{13}	10^{12}
$\mu_e\tau_e$ (cm^2/V)	>1	>1	10^{-5}	10^{-3}	10^{-3} - 10^{-2}	10^{-4}	10^{-5}
$\mu_h\tau_h$ (cm^2/V)	≈ 1	>1	10^{-6}	10^{-4}	10^{-5}	10^{-5}	10^{-6}

The more common growth methods: C = Czochralski, CVD = Chemical Vapor Deposition, THM = Traveling Heater Method, BM = Bridgman Method, HPB = High-Pressure Bridgman and VAM = Vertical Ampoule Method, $\mu_e\tau_e$ and $\mu_h\tau_h$ are the electron- and hole mobility-lifetimes.

Bibliography

Alvarez, Jose-Manuel, Jose Luis Galvez, Margarita Hernanz, Jordi Isern, Manuel Lozano, Giulio Pellegrini, Mokhtar Chmeissani, Ezio Caroli, and Rui M Curado da Silva (2011). "CdTe/ CZT pixel detector for gamma-ray spectrometry with imaging and polarimetry capability in astrophysics". In: *2011 IEEE Nuclear Science Symposium and Medical Imaging Conference (2011 NSS/MIC)*. IEEE, pp. 4611–4615.

Amptek Inc. (2002). *Efficiency of Amptek XR-100T-CdTe and - CZT Detectors Application Note ANCZT-1 Rev 2.* Online; accessed 13-January-2017. URL: http://amptek.com/pdf/cztapp1.pdf.

— (2016). *Website of the Amptek company.* Online; accessed 13-January-2017. URL: http://amptek.com.

— (2017). *Website of a Si-PIN detector from the Amptek company*. Online; accessed 12-May-2017. URL: http://amptek.com/products/xr-100cr-si-pin-x-ray-detector/.

Auterinen, Iiro, Pekka Hiismäki, Petri Kotiluoto, Rolf J. Rosenberg, Seppo Salmenhaara, Tiina Seppälä, Tom Serén, Vesa Tanner, Carita Aschan, Mika Kortesniemi, Antti Kosunen, Juhad Lampinen, Sauli Savolainen, Matti Toivonen, and Petteri Välimäki (2001). "Metamorphosis of a 35 Year-Old TRIGA Reactor into a Modern BNCT Facility". In: *Frontiers in Neutron Capture Therapy: Volume 1*. Ed. by M. Frederick Hawthorne, Kenneth Shelly, and Richard J. Wiersema. Boston, MA: Springer US, pp. 267–275. ISBN: 978-1-4615-1285-1. DOI: 10.1007/978-1-4615-1285-1_36. URL: http://dx.doi.org/10.1007/978-1-4615-1285-1_36.

Barber, W C, J C Wessel, E Nygard, and J S Iwanczyk (2015). "Energy dispersive CdTe and CdZnTe detectors for spectral clinical CT and NDT applications". In: *Nuclear Instruments*

and Methods in Physics Research Section A: Accelerators, Spectrometers, Detectors and Associated Equipment 784, pp. 531–537.

Beckert, M Brooke, Sabrina Gallego, Yong Ding, Eric Elder, and Jason H Nadler (2016). "Medical imaging scintillators from glass-ceramics using mixed rare-earth halides". In: *Optical Materials* 60, pp. 513–520.

Biomedicum Helsinki Foundation (2016). *Helsinki University Hospital receives a novel type of neutron source for cancer therapy*. Online; accessed 2-April-2017. URL: http://www.biomedicum.fi/index.php?page=2826&lang=2.

Bushberg, Jerrold T., J. Anthony Seibert, Edwin M. Leidholdt, and John M. Boone (2001). *The Essential Physics of Medical Imaging (2nd Edition)*. 2nd ed. Lippincott Williams & Wilkins. ISBN: 0683301187.

Casten, R F, J Jolie, H G Börner, D S Brenner, N V Zamfir, W T Chou, and A Aprahamian (1992). "The enigma of 114Cd. A classical case of ambiguities in quantum mechanical state mixing". In: *Physics Letters B* 297.1-2, pp. 19–24.

Chadwick, M.B., M. Herman, P. Obložinský, M.E. Dunn, Y. Danon, A.C. Kahler, D.L. Smith, B. Pritychenko, G. Arbanas, R. Arcilla, R. Brewer, D.A. Brown, R. Capote, A.D. Carlson, Y.S. Cho, H. Derrien, K. Guber, G.M. Hale, S. Hoblit, S. Holloway, T.D. Johnson, T. Kawano, B.C. Kiedrowski, H. Kim, S. Kunieda, N.M. Larson, L. Leal, J.P. Lestone, R.C. Little, E.A. McCutchan, R.E. MacFarlane, M. MacInnes, C.M. Mattoon, R.D. McKnight, S.F. Mughabghab, G.P.A. Nobre, G. Palmiotti, A. Palumbo, M.T. Pigni, V.G. Pronyaev, R.O. Sayer, A.A. Sonzogni, N.C. Summers, P. Talou, I.J. Thompson, A. Trkov, R.L. Vogt, S.C. van der Marck, A. Wallner, M.C. White, D. Wiarda, and P.G. Young (2011). "ENDF/B-VII.1 Nuclear Data for Science and Technology: Cross Sections, Covariances, Fission Product Yields and Decay Data". In: *Nuclear Data Sheets* 112.12. Special Issue on ENDF/B-VII.1 Library, pp. 2887 –2996. ISSN: 0090-3752. DOI: 10.1016/j.nds.2011.11.002. URL: http://www.sciencedirect.com/science/article/pii/S009037521100113X.

Coderre, Jeffrey A, Arjun D Chanana, Darrel D Joel, Eric H Elowitz, Peggy L Micca, Marta M Nawrocky, Manjeet Chadha, Jan-Olaf Gebbers, Magdy Shady, Nancy S Peress, and Daniel N Slatkin (1998). "Biodistribution of

Boronophenylalanine in Patients with Glioblastoma Multiforme: Boron Concentration Correlates with Tumor Cellularity". In: *Radiation Research* 149.2, p. 163.

Del Sordo, Stefano, Leonardo Abbene, Ezio Caroli, Anna Maria Mancini, Andrea Zappettini, and Pietro Ubertini (2009). "Progress in the Development of CdTe and CdZnTe Semiconductor Radiation Detectors for Astrophysical and Medical Applications". In: *Sensors* 9 (5), pp. 3491–3526.

DeMarco, John J, Robert E Wallace, and Kirsten Boedeker (2002). "An analysis of MCNP cross-sections and tally methods for low-energy photon emitters". In: *Physics in Medicine and Biology* 47.8, pp. 1321–1332.

Dominguez, A, D Abbaneo, K Arndt, N Bacchetta, A Ball, E Bartz, W Bertl, G M Bilei, G Bolla, H W K Cheung, M Chertok, S Costa, N Demaria, Daniel Dominguez Vazquez, K Ecklund, W Erdmann, K Gill, G Hall, K Harder, F Hartmann, R Horisberger, W Johns, H C Kaestli, K Klein, D Kotlinski, S Kwan, M Pesaresi, H Postema, T Rohe, C Schäfer, A Starodumov, S Streuli, A Tricomi, P Tropea, J Troska, F Vasey, and W Zeuner (2012). *CMS Technical Design Report for the Pixel Detector Upgrade*. Tech. rep. CERN-LHCC-2012-016. CMS-TDR-11. URL: `http://cds.cern.ch/record/1481838`.

El Kanawati, W, B Perot, C Carasco, C Eleon, V Valkovic, D Sudac, J Obhodas, and G Sannie (2011). "Acquisition of prompt gamma-ray spectra induced by 14MeV neutrons and comparison with Monte Carlo simulations". In: *Applied Radiation and Isotopes* 69.5, pp. 732–743.

Eremin, V, N Strokan, E Verbitskaya, and Z Li (1996). "Development of transient current and charge techniques for the measurement of effective net concentration of ionized charges (Neff) in the space charge region of p-n junction detectors". In: *Nuclear Instruments and Methods in Physics Research Section A: Accelerators, Spectrometers, Detectors and Associated Equipment* 372.3, pp. 388–398.

Hasegawa, Bruce H, Benno Stebler, Brian K Rutt, Alberto Martinez, Eric L Gingold, Craig S Barker, Kenneth G Faulkner, Christopher E Cann, and Douglas P Boyd (1991). "A prototype high-purity germanium detector system with fast photon-counting circuitry for medical imaging". In: *Medical Physics* 18.5, pp. 900–909.

Hassanein, Rene, Eberhard Lehmann, and Peter Vontobel (2005). "Methods of scattering corrections for quantitative neutron radiography". In: *Nuclear Instruments and Methods in Physics Research Section A: Accelerators, Spectrometers, Detectors and Associated Equipment* 542.1-3, pp. 353–360.

Horiike, H, I Murata, T Iida, S Yoshihashi, E Hoashi, I Kato, N Hashimoto, S Kuri, and S Oshiro (2015). "Liquid Li based neutron source for BNCT and science application". In: *Applied Radiation and Isotopes* 106, pp. 92–94.

IAEA (2007). *Database of Prompt Gamma Rays from Slow Neutron Capture for Elemental Analysis*. Non-serial Publications. Online; accessed 13-January-2017. URL: http://www-pub.iaea.org/MTCD/Publications/PDF/Pub1263_web.pdf.

ILO, International Labour Organization (1960). *Radiation Protection Convention C115*. Online; accessed 7-May-2017. URL: http://www.ilo.org/dyn/normlex/en/f?p=NORMLEXPUB:12100:0::NO::P12100_ILO_CODE:C115.

Jeong, Manhee, Han Soo Kim, Young Soo Kim, and Jang Ho Ha (2014). "Characteristics of a planar-type Cd0.9Zn0.1Te radiation detector grown by using the low-pressure bridgman method". In: *Journal of the Korean Physical Society* 64.8, pp. 1105–1109. ISSN: 1976-8524. DOI: 10.3938/jkps.64.1105. URL: http://dx.doi.org/10.3938/jkps.64.1105.

Kalender, Willi A, Daniel Kolditz, Christian Steiding, Veikko Ruth, Ferdinand Lück, Ann-Christin Rößler, and Evelyn Wenkel (2016). "Technical feasibility proof for high-resolution low-dose photon-counting CT of the breast". In: *European Radiology* 27.3, pp. 1081–1086.

Kankaanranta, Leena, Tiina Seppälä, Hanna Koivunoro, Kauko Saarilahti, Timo Atula, Juhani Collan, Eero Salli, Mika Kortesniemi, Jouni Uusi-Simola, Petteri Välimäki, Antti Mäkitie, Marko Seppänen, Heikki Minn, Hannu Revitzer, Mauri Kouri, Petri Kotiluoto, Tom Seren, Iiro Auterinen, Sauli Savolainen, and Heikki Joensuu (2012). "Boron Neutron Capture Therapy in the Treatment of Locally Recurred Head-and-Neck Cancer: Final Analysis of a Phase I/II Trial". In: *International Journal of Radiation Oncology*Biology*Physics* 82.1, e67–e75.

Kargar, Alireza, Mark J Harrison, Adam C Brooks, and Douglas S McGregor (2010). "Characterization of charge carrier collection in a CdZnTe Frisch collar detector with a highly collimated source". In: *Nuclear Instruments and Methods in Physics Research Section A: Accelerators, Spectrometers, Detectors and Associated Equipment* 620.2-3, pp. 270–278.

Knoll, Glenn (2010). *Radiation detection and measurement*. 4th. Hoboken, N.J: John Wiley. ISBN: 978-0-470-13148-0.

Kobayashi, Tooru, Yoshinori Sakurai, and Masayori Ishikawa (2000). "A noninvasive dose estimation system for clinical BNCT based on PG-SPECT—Conceptual study and fundamental experiments using HPGe and CdTe semiconductor detectors". In: *Medical Physics* 27.9, p. 2124.

Koivunoro, Hanna, Teemu Siiskonen, Petri Kotiluoto, Iiro Auterinen, Eero Hippeläinen, and Sauli Savolainen (2012). "Accuracy of the electron transport in mcnp5 and its suitability for ionization chamber response simulations: A comparison with the egsnrc and penelope codes". In: *Medical Physics* 39.3, pp. 1335–1344.

Koning, A J and D Rochman (2012). "Modern Nuclear Data Evaluation with the TALYS Code System". In: *Nuclear Data Sheets* 113.12, pp. 2841–2934.

Koning, A.J. and D. Rochman (2008). *TENDL-2008: "TALYS-based Evaluated Nuclear Data Library"*. Nuclear Research and Consultancy Group (NRG), Petten, The Netherlands. Online; accessed 13-January-2017. URL: `http://www.talys.eu/tendl-2008/`.

Kreiner, A J, M Baldo, J R Bergueiro, D Cartelli, W Castell, V Thatar Vento, J Gomez Asoia, D Mercuri, J Padulo, J C Suarez Sandin, J Erhardt, J M Kesque, A A Valda, M E Debray, H R Somacal, M Igarzabal, D M Minsky, M S Herrera, M E Capoulat, S J Gonzalez, M F del Grosso, L Gagetti, M Suarez Anzorena, M Gun, and O Carranza (2014). "Accelerator-based BNCT". In: *Applied Radiation and Isotopes* 88, pp. 185–189.

Kumada, H, A Matsumura, and H Sakurai (2011). "New challenge for advanced BNCT in University of Tsukuba. In the front edge of BNCT development." In: *Proceedings of Sixth Young Researchers BNCT Meeting*. YBNCT, pp. 132–6. ISBN: 978-986-03-0321-6.

Li, Zaoyang, Jeffrey H Peterson, Andrew Yeckel, and Jeffrey J Derby (2016). "Analysis of the effects of a rotating magnetic field on the growth of cadmium zinc telluride by the traveling heater method under microgravity conditions". In: *Journal of Crystal Growth* 452, pp. 17–21.

Locher, G.L. (1936). "Biological effects and therapeutic possibilities of neutrons". In: *Am. J. Roentgenol. Radium Ther* 36, pp. 1–13.

Los Alamos National Laboratory (2004). *MCB-DLC200*. Includes the ENDL92 nuclear data library. URL: https://www.oecd-nea.org/tools/abstract/detail/dlc-0200.

Macias-Montero, Jose-Gabriel, Maher Sarraj, Mokhtar Chmeissani, Ricardo Martinez, and Carles Puigdengoles (2015). "A 2D 4x4 Channel Readout ASIC for Pixelated CdTe Detectors for Medical Imaging Applications". In: *IEEE Transactions on Nuclear Science* 62.5, pp. 2327–2333.

Mikhaylova, Ekaterina, Gianluca De Lorenzo, Mokhtar Chmeissani, Machiel Kolstein, Mario Canadas, Pedro Arce, Yonatan Calderon, Dilber Uzun, Gerard Arino, Jose-Gabriel Macias-Montero, Ricardo Martinez, Carles Puigdengoles, and Enric Cabruja (2013). "Simulation of the Expected Performance of a Seamless Scanner for Brain PET Based on Highly Pixelated CdTe Detectors". In: *IEEE Transactions on Medical Imaging* 33.2, pp. 332–339.

Minsky, D M, A A Valda, A J Kreiner, S Green, C Wojnecki, and Z Ghani (2009). "Experimental feasibility studies on a SPECT tomograph for BNCT dosimetry". In: *Applied Radiation and Isotopes* 67.7-8, S.179 –S182.

— (2011). "First tomographic image of neutron capture rate in a BNCT facility". In: *Applied Radiation and Isotopes* 69.12, pp. 1858–1861.

Mishima, Yutaka, Chihiro Honda, Masamitsu Ichihashi, Hidefumi Obara, Junichi Hiratsuka, Hiroshi Fukuda, Hiroshi Karashima, Tooru Kobayashi, Keiji Kanda, and Kazuo Yoshino (1989). "TREATMENT OF MALIGNANT MELANOMA BY SINGLE THERMAL NEUTRON CAPTURE THERAPY WITH MELANOMA-SEEKING 10B-COMPOUND". In: *The Lancet* 334.8659, pp. 388–389.

Moll, M, E Fretwurst, and G Lindström (1999). "Leakage current of hadron irradiated silicon detectors – material dependence". In: *Nuclear Instruments and Methods in Physics Research Section A: Accelerators, Spectrometers, Detectors and Associated Equipment* 426.1, pp. 87–93.

Monshizadeh, M, Y Kasesaz, H Khalafi, and S Hamidi (2015). "MCNP design of thermal and epithermal neutron beam for BNCT at the Isfahan MNSR". In: *Progress in Nuclear Energy* 83, pp. 427–432.

Monte Carlo Team (2003a). *X-5 Monte Carlo Team, "MCNP - A General N-Particle Transport Code, Version 5"*. Report No. LA-UR-03-1987.

— (2003b). *X-5 Monte Carlo Team, "MCNP - A General N-Particle Transport Code, Version 5"*. Report No. LA-CP-03-0245.

— (2005). *X-5 Monte Carlo Team, "MCNP - A General N-Particle Transport Code, Version 5"*. URL: https://laws.lanl.gov/vhosts/mcnp.lanl.gov/mcnp5.shtml.

Mueller, Jennifer L. and Samuli Siltanen (2012). *Linear and Nonlinear Inverse Problems with Practical Applications*. Vol. 10. Computational science and engineering. SIAM. ISBN: 978-1-61197-233-7. DOI: 10.1137/1.9781611972344. URL: http://dx.doi.org/10.1137/1.9781611972344.

Muenzel, Daniela, Daniel Bar-Ness, Ewald Roessl, Ira Blevis, Matthias Bartels, Alexander A Fingerle, Stefan Ruschke, Philippe Coulon, Heiner Daerr, Felix K Kopp, Bernhard Brendel, Axel Thran, Michal Rokni, Julia Herzen, Loic Boussel, Franz Pfeiffer, Roland Proksa, Ernst J Rummeny, Philippe Douek, and Peter B Noël (2016). "Spectral Photon-counting CT: Initial Experience with Dual–Contrast Agent K-Edge Colonography". In: *Radiology*, p. 160890.

Murata, Isao, Soichiro Nakamura, Masanobu Manabe, Hiroyuki Miyamaru, and Itsuro Kato (2014). "Characterization measurement of a thick CdTe detector for BNCT-SPECT – Detection efficiency and energy resolution". In: *Applied Radiation and Isotopes* 88.C, pp. 129–133.

Nakagawa, Yoshinobu and Hiroshi Hatanaka (1997). "Boron neutron capture therapy: Clinical brain tumor studies". In: *Journal of Neuro-Oncology* 33.1-2, pp. 105–115.

Nikl, Martin (2006). "Scintillation detectors for x-rays". In: *Measurement Science and Technology* 17.4, R37–R54.

NIST (2017). *XCOM: Photon Cross Sections Database. Physical Measurement Laboratory*. URL: https://www.nist.gov/pml/xcom-photon-cross-sections-database.

NNDC, National Nuclear Data Center and Brookhaven National Labratory BNL (2017). *Thermal Neutron Capture Gammas — Target Nucleus ^{113}Cd*. Internet database. Online; accessed 13-January-2017. URL: http://www.nndc.bnl.gov/capgam/byn/page128.html.

OECD (2017). *OECD Nuclear Energy Agency*. Online; accessed 13-January-2017. URL: https://www.oecd-nea.org.

Pani, R, M Colarieti-Tosti, M N Cinti, C Polito, C Trigila, and S Ridolfi (2016). "Investigation of radiation detection properties of CRY-018 and CRY-019 scintillators for medical imaging". In: *Journal of Instrumentation* 11.09, P09010–P09010.

Phoenix, B, S Green, M C Scott, J R J Bennett, and T R Edgecock (2015). "Development of a higher power cooling system for lithium targets". In: *Applied Radiation and Isotopes* 106, pp. 49–52.

Pourmorteza, Amir, Rolf Symons, Veit Sandfort, Marissa Mallek, Matthew K Fuld, Gregory Henderson, Elizabeth C Jones, Ashkan A Malayeri, Les R Folio, and David A Bluemke (2016). "Abdominal Imaging with Contrast-enhanced Photon-counting CT: First Human Experience". In: *Radiology* 279.1, pp. 239–245.

Redus, R., A Huber, J Pantazis, T Pantazis, and D Sperry (2006). "Design and performance of the X-123 compact X-ray and gamma-ray spectroscopy system". In: *2006 IEEE Nuclear Science Symposium Conference Record*. IEEE, pp. 3794–3797.

Riley George, A. and Steven Bornstein (2001). "Room temperature flip chip assembly of CdZnTe pixel detector arrays". In: High-density interconnect and systems packaging. (Apr. 17–20, 2001). Online; accessed 8-May-2017. Santa Clara CA: Society of Photo-Optical Instrumentation Engineers. ISBN: 0-8194-4139-2. URL: http://cat.inist.fr/?aModele=afficheN&cpsidt=1020928.

Roessl, E and R Proksa (2007). "K-edge imaging in x-ray computed tomography using multi-bin photon counting detectors". In: *Physics in Medicine and Biology* 52.15, pp. 4679–4696.

Rosenschöld, P M Munck af, W F A R Verbakel, C P Ceberg, F Stecher-Rasmussen, and B R R Persson (2001). "Toward clinical application of prompt gamma spectroscopy for in vivo

monitoring of boron uptake in boron neutron capture therapy". In: *Medical Physics* 28.5, p. 787.

Särkkä, S. (2013). *Bayesian Filtering and Smoothing*. Cambridge University Press. ISBN: 9781107619289.

Savolainen, Sauli, Mika Kortesniemi, Marjut Timonen, Vappu Reijonen, Linda Kuusela, Jouni Uusi-Simola, Eero Salli, Hanna Koivunoro, Tiina Seppälä, Nadja Lönnroth, Petteri Välimäki, Heini Hyvönen, Petri Kotiluoto, Tom Seren, Antti Kuronen, Sami Heikkinen, Antti Kosunen, and Iiro Auterinen (2013). "Boron neutron capture therapy (BNCT) in Finland: Technological and physical prospects after 20 years of experiences". In: *Physica Medica* 29.3, pp. 233–248.

Scheel, Hans J. and Tsuguo Fukuda (2009). *Crystal Growth Technology*. Online; accessed 12-May-2017. Wiley. ISBN: 97804714-90593. URL: http://onlinelibrary.wiley.com/book/10.1002/0470871687.

Schlomka, J P, E Roessl, R Dorscheid, S Dill, G Martens, T Istel, C Bäumer, C Herrmann, R Steadman, G Zeitler, A Livne, and R Proksa (2008). "Experimental feasibility of multi-energy photon-counting K-edge imaging in pre-clinical computed tomography". In: *Physics in Medicine and Biology* 53.15, pp. 4031–4047.

Shibata, Keiichi, Osamu Iwamoto, Tsuneo Nakagawa, Nobuyuki Iwamoto, Akira Ichihara, Satoshi Kunieda, Satoshi Chiba, Kazuyoshi Furutaka, Naohiko Otuka, Takaaki Ohasawa, Toru Murata, Hiroyuki Matsunobu, Atsushi Zukeran, So Kamada, and Jun-ichi Kayakura (2012). "JENDL-4.0: A New Library for Nuclear Science and Engineering". In: *Journal of Nuclear Science and Technology*.

Shikhaliev, Polad M and Shannon G Fritz (2011). "Photon counting spectral CT versus conventional CT: comparative evaluation for breast imaging application". In: *Physics in Medicine and Biology* 56.7, pp. 1905–1930.

Slatkin, D.N. (1991). "A history of boron neutron capture therapy of brain tumours. Postulation of a brain radiation dose tolerance limit". In: *Brain* 114, pp. 1609–21.

Stahle, C M, B H Parker, A M Parsons, L M Barbier, S D Barthelmy, N A Gehrels, D M Palmer, S J Snodgrass, and J Tueller (1999). "CdZnTe and CdTe detector arrays for hard X-ray and gamma-ray astronomy". In: *Nuclear Instruments*

and Methods in Physics Research Section A: Accelerators, Spectrometers, Detectors and Associated Equipment 436.1-2, pp. 138–145.

Su, Ching-Hua (2015). "A method of promoting single crystal yield during melt growth of semiconductors by directional solidification". In: *Journal of Crystal Growth* 410, pp. 35–38.

Sun, Y., J. Faucher, D. Jung, M. Vaisman, C. McPheeters, P. Sharps, E. Perl, J. Simon, M. Steiner, D. Friedman, and M. L. Lee (2016). "Thermal stability of GaAs solar cells for high temperature applications". In: *2016 IEEE 43rd Photovoltaic Specialists Conference (PVSC)*, pp. 2385–2388. DOI: 10.1109/PVSC.2016.7750068.

Symons, Rolf, Tyler E Cork, Pooyan Sahbaee, Matthew K Fuld, Steffen Kappler, Les R Folio, David A Bluemke, and Amir Pourmorteza (2017). "Low-dose lung cancer screening with photon-counting CT: a feasibility study". In: *Physics in Medicine and Biology* 62.1, pp. 202–213.

Sze, Simon M. and Kwok K. Ng (2006). *Physics of Semiconductor Devices*. Wiley-Interscience. ISBN: 0471143235. URL: http://onlinelibrary.wiley.com/book/10.1002/04700\-68329.

Szeles, Csaba, Derek Bale, Joseph Grosholz Jr., Gary L. Smith, Michael Blostein, and John Eger (2006). "Fabrication of high-performance CdZnTe quasi-hemispherical gamma-ray CAPture plus detectors". In: vol. 6319, pp. 631909–631909–9. DOI: 10.1117/12.683552. URL: http://dx.doi.org/10.1117/12.683552.

Takahashi, T, T Mitani, Y Kobayashi, M Kouda, G Sato, S Watanabe, K Nakazawa, Y Okada, M Funaki, R Ohno, and K Mori (2002). "High-resolution Schottky CdTe diode detector". In: *IEEE Transactions on Nuclear Science* 49.3, pp. 1297–1303.

Tanaka, H, Y Sakurai, M Suzuki, S Masunaga, T Mitsumoto, K Fujita, G Kashino, Y Kinashi, Y Liu, M Takada, K Ono, and A Maruhashi (2011). "Experimental verification of beam characteristics for cyclotron-based epithermal neutron source (C-BENS)". In: *Applied Radiation and Isotopes* 69.12, pp. 1642–1645.

Valda, A, D M Minsky, A J Kreiner, A A Burlon, and H Somacal (2005). "Development of a tomographic system for online dose measurements in BNCT (Boron Neutron Capture Therapy)". In: *Brazilian Journal of Physics* 35.3B, pp. 785–788.

Varshni, Y P (1967). "Temperature dependence of the energy gap in semiconductors". In: *Physica* 34.1, pp. 149–154.

Verbakel, W F A R and F Stecher-Rasmussen (1997). "A γ-ray telescope for on-line measurements of low boron concentrations in a head phantom for BNCT". In: *Nuclear Instruments and Methods in Physics Research Section A: Accelerators, Spectrometers, Detectors and Associated Equipment* 394.1-2, pp. 163–172.

Wang, Xiaolan, Dirk Meier, Katsuyuki Taguchi, Douglas J Wagenaar, Bradley E Patt, and Eric C Frey (2011). "Material separation in x-ray CT with energy resolved photon-counting detectors". In: *Medical Physics* 38.3, pp. 1534–1546.

Wei, S.-H. and S.B. Zhang (2001). "Theoretical Study of Doping Limits of CdTe". In: NCPV Program Review Meeting. (2001).

Wikipedia (2017). *Neutron capture therapy of cancer — Wikipedia, The Free Encyclopedia*. Online; accessed 13-January-2017. URL: https://en.wikipedia.org/w/index.php?title=Neutron_capture_therapy_of_cancer&oldid=758\-650459.

Wilson, Matthew D, Steven J Bell, Robert J Cernik, Christiana Christodoulou, Christopher K Egan, Daniel O'Flynn, Simon Jacques, Silvia Pani, James Scuffham, Paul Seller, Paul J Sellin, Robert Speller, and Matthew C Veale (2013). "Multiple Module Pixellated CdTe Spectroscopic X-Ray Detector". In: *IEEE Transactions on Nuclear Science* 60.2, pp. 1197–1200.

Winkler, Alexander (2017). "Comparison of characterization methods for CdTe/ CdZnTe radiation detector materials and development of an automated test system". Diplomarbeit, Friedrich - Schiller - Universität Jena, 2011. Jena. URL: https://www.db-thueringen.de/receive/dbt_mods_00031853.

Wu, X, P Kostamo, A Gädda, S Nenonen, T Riekkinen, J Härkönen, J Salonen, H Andersson, Y Zhilyaev, L Fedorov, S Eranen, M Mattila, H Lipsanen, M Prunnila, J Kalliopuska, and A Oja (2014). " Radiation detectors fabricated on high-purity GaAs epitaxial materials". In: *Journal of Instrumentation* 9.12, pp. C12024–C12024.

Ye, Sung-Joon, Ivan A Brezovich, Prem Pareek, and Shahid A Naqvi (2004). "Benchmark of PENELOPE code for low-energy photon transport: dose comparisons with MCNP4

and EGS4". In: *Physics in Medicine and Biology* 49.3, pp. 387–397.

Yonenaga, Ichiro, Utako Onose, and Koji Sumino (1987). "Mechanical properties of GaAs crystals". In: *Journal of Materials Research* 2.2, 252–261. DOI: 10.1557/JMR.1987.0252.

Yu, Z, S Leng, S M Jorgensen, Z Li, R Gutjahr, B Chen, X Duan, A F Halaweish, L Yu, E L Ritman, and C H McCollough (2015). "Initial results from a prototype whole-body photon-counting computed tomography system". In: *SPIE Medical Imaging*. Ed. by Christoph Hoeschen, Despina Kontos, and Thomas G Flohr. SPIE, 94120W–14.

Zhang, Zhenyu, Hang Gao, Wanqi Jie, Dongming Guo, Renke Kang, and Yan Li (2008). "Chemical mechanical polishing and nanomechanics of semiconductor CdZnTe single crystals". In: *Semiconductor Science and Technology* 23.10, p. 105023.